Contrib Mineral Petrol (2014) 167:1002
DOI 10.1007/s00410-014-1002-x

ORIGINAL PAPER

Geochemistry of ultrahigh-pressure anatexis: fractionation of elements in the Kokchetav gneisses during melting at diamond-facies conditions

Aleksandr S. Stepanov · Joerg Hermann · Andrey V. Korsakov · Daniela Rubatto

Received: 4 November 2013 / Accepted: 25 March 2014

Abstract The Kokchetav complex in Kazakhstan contains garnet-bearing gneisses that formed by partial melting of metasedimentary rocks at ultrahigh-pressure (UHP) conditions. Partial melting and melt extraction from these rocks is documented by a decrease in K_2O and an increase in FeO + MgO in the restites. The most characteristic trace element feature of the Kokchetav UHP restites is a strong depletion in light rare earth elements (LREE), Th and U. This is attributed to complete dissolution of monazite/allanite in the melt and variable degree of melt extraction. In contrast, Zr concentrations remain approximately constant in all gneisses. Using experimentally determined solubilities of LREE and Zr in high-pressure melts, these data constrain the temperature of melting to ~1,000 °C. Large ion lithophile elements (LILE) are only moderately depleted in the samples that have the lowest U, Th and LREE contents, indicating that phengite retains some LILE in the residue. Some restites display an increase in Nb/Ta with respect to the protolith. This further suggests the presence of phengite, which, in contrast to rutile, preferentially incorporates Nb over Ta. The trace element fractionation observed during UHP anatexis in the Kokchetav gneisses is significantly different from depletions reported in low-pressure restites, where generally no LREE and Th depletion occurs. Melting at UHP conditions resulted in an increase in the Sm/Nd ratio and a decoupling of the Sm–Nd and Lu–Hf systems in the restite. Further subduction of such restites and mixing with mantle rocks might thus lead to a distinct isotopic reservoir different from the bulk continental crust.

Keywords Anatexis · UHP metamorphism · REE · Accessory minerals

Communicated by J. Hoefs.

A. S. Stepanov (✉) · J. Hermann · D. Rubatto
Research School of Earth Sciences, The Australian National University, Mills Road, Bld. 61, Canberra, ACT 0200, Australia
e-mail: sashas@utas.edu.au

Present Address:
A. S. Stepanov
ARC Centre of Excellence in Ore Deposits (CODES), School of Physical Sciences, University of Tasmania, Private Bag 79, Hobart, Tasmania 7001, Australia

A. V. Korsakov
V.S. Sobolev Institute of Geology and Mineralogy of Siberian Branch of Russian Academy of Science, Koptyug Pr. 3, Novosibirsk 630090, Russia

A. V. Korsakov
Novosibirsk State Univesity, 2 Pirogova Str., Novosibirsk-90 630090, Russia

Introduction

At active plate margins, the crust and its sedimentary cover are subducted into the mantle and undergo heating, dehydration, mixing with mantle material and partial melting. This is one of the major processes for the recycling back into the mantle of incompatible elements that are enriched in the crust (Zindler and Hart 1986; Plank and Langmuir 1998). The composition and volume of sediments, oceanic crust and suboceanic lithosphere constrain the input, whereas magmas emitted to the surface represent the output of subduction zones. The comparison of trace element characteristics of input and output materials suggested that sediments play a major role in this large–scale recycling (Plank and Langmuir 1998). Metasediments are the most fertile components of the subducted lithosphere, and they

Published online: 16 April 2014

have the lowest melting temperature and are thus able to melt to a high extent during subduction. The composition of major and trace elements liberated from sediment melting can be investigated experimentally (Schmidt et al. 2004b; Auzanneau et al. 2006; Hermann and Spandler 2008; Hermann and Rubatto 2009; Skora and Blundy 2010; Martindale et al. 2013). However, in order to understand the complex processes of melting and melt extraction, experimental data must be complemented with field studies of high-pressure rocks, where these processes occurred on a larger scale.

Bulk rock compositions of deeply subducted crustal material provide first-order information on the efficiency of element fractionation during fluid–rock interaction. The effect of metamorphism on bulk rock compositions of eclogite facies rocks has been investigated in numerous studies (Bebout et al. 1993, 1999, 2007; Shatsky et al. 1999; Spandler et al. 2003; John et al. 2004; Volkova et al. 2009; Zheng et al. 2011). These works demonstrated that fluid/melt loss and mobility results in a redistribution of fluid mobile elements during eclogite facies metamorphism. However, many lithophile trace elements often remain unaffected by subduction even at ultrahigh-pressure (UHP) conditions up to 40 kbar and 700 °C (Bebout et al. 1993, 1999, 2007; Hermann 2002; Spandler et al. 2003; Zheng et al. 2011). Thus, significant changes in major and trace element compositions are restricted to UHP rocks that experienced extensive melting at high temperatures of 900–1,000 °C (Hermann and Rubatto 2014). In order to understand element redistribution by partial melting in UHP rocks, it is essential to consider the main mineral hosts for the trace elements of interest. Accessory phases play a crucial role for many of these trace elements. For example, allanite and monazite are the main hosts for LREE, Th and U (Hermann 2002; Skora and Blundy 2010), whereas rutile has been considered a main host for Nb and Ta (Rudnick et al. 2000; Hermann and Rubatto 2009; Zheng et al. 2011). Experimental studies have shown that the solubility in melts of elements that are essential structural components of accessory minerals, such as Ce in monazite and Zr in zircon, is a strong function of temperature (Watson and Harrison 1983). Therefore, the temperature of melting and the amount of melt extraction combined with the original content of these elements in the protolith will determine whether these elements are enriched or depleted during the melting process. The distribution of trace elements that are not essential structural components of minerals such as Nb and Ta will be governed by partitioning between residual minerals and the melt. Therefore, bulk rock compositions of UHP rocks in conjunction with residual mineralogy of the rocks and combined with experimental information on solubility and partitioning provide valuable information on processes of element redistribution during partial melting in subducted sediments.

The Kokchetav complex in Kazakhstan is ideal for the study of UHP melting, as these rocks experienced peak conditions of 45–60 kbar and 950–1,000 °C (Sobolev and Shatsky 1990; Hermann et al. 2001; Auzanneau et al. 2010; Mikhno and Korsakov 2013; Schertl and Sobolev 2013). Partial melting of the Kokchetav rocks was proposed on the basis of bulk rock geochemistry (Shatsky et al. 1995, 1999, 2006), reaction textures (Korsakov et al. 2004, 2006) and presence of melt inclusions (Korsakov and Hermann 2006; Hwang et al. 2006; Mikhno et al. 2013). This study presents new data on bulk rock major and trace element compositions of the metasedimentary rocks of the Kokchetav complex. In order to quantify the mobility of major and trace elements during UHP metamorphism, the compositions of gneisses from UHP terrains are compared with non-UHP samples from various parts of the Kokchetav complex, considered as potential protoliths for UHP gneisses. The composition of the UHP gneisses is interpreted in light of recent experimental studies (Hermann and Rubatto 2009; Skora and Blundy 2010, 2012; Stepanov et al. 2012; Stepanov and Hermann 2013) providing first-order constraints on the melting history, mineral assemblages and relative fractionation of elements during UHP melting.

Geological background

The Kokchetav metamorphic complex (also known as Kokchetav metamorphic belt—KMB or Kokchetav massif) is located in northern Kazakhstan about 270 km northwest from Astana, the new capital of Kazakhstan and 900 km west of Novosibirsk, a major city in Siberia, Russia (Fig. 1). The Kokchetav metamorphic belt is located in the central part of Eurasia within the large Palaeozoic Central Asia Fold Belt. The Kokchetav complex is composed of rock units, which experienced different metamorphic conditions that have been named suites, domains and/or terrains (Rozen 1971; Dobretsov et al. 1995; Kaneko et al. 2000; Theunissen et al. 2000a, b; Glorie et al. 2013). From east to west, there are several localities where UHP rocks are exposed: Kulet, Kumdy-Kol and Barchi-Kol. Kumdy-Kol and Barchi-Kol reached sufficiently high pressures to stabilize metamorphic diamond and peak temperatures are estimated at 950–1,000 °C (Sobolev and Shatsky 1990; Hermann et al. 2001; Schertl and Sobolev 2013), whereas in the Kulet area, metamorphism occurred in the stability field of coesite ($P > 30$ kbar) and at lower temperatures of 720–760 °C (Shatsky et al. 1998; Parkinson 2000; Theunissen et al. 2000a). These terrains are surrounded by units consisting of eclogite facies rocks that display lower peak metamorphic conditions. The juxtaposition of HP and UHP rocks is interpreted as mega-melange (Dobretsov

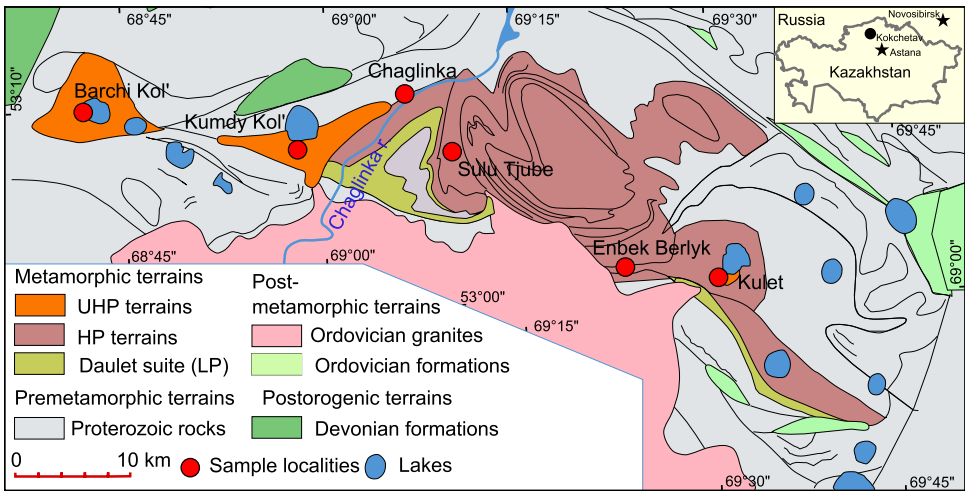

Fig. 1 General structure of the Kokchetav complex simplified from the map by Zhimulev (2007). The locations of the samples are indicated. For the coloured version of this and following figures, the reader is referred to the electronic version of the paper

et al. 1995, 2006; Theunissen et al. 2000b; Zhimulev et al. 2010, 2011) or as stacking of units in a subduction channel (Kaneko et al. 2000; Masago 2000). The Daulet suite outcrops in the vicinity of the UHP rocks and experienced low pressure–high temperature metamorphism. This suite is interpreted as a contact metamorphic overprint related to the emplacement either of hot UHP rocks at mid-crustal levels (Kaneko et al. 2000; Terabayashi et al. 2002; Buslov et al. 2010) or Zrenda granite batolith (Reverdatto et al. 1993).

The UHP blocks are composed mostly of garnet-rich gneisses with eclogite lenses but also contain more exotic lithologies: white schists in Kulet, garnet pyroxenites with high diamond content and high-K pyroxenes in Kumdy-Kol (Mikhno and Korsakov 2013), UHP marbles (Ogasawara et al. 2000, 2002) and zoisite gneiss with diamonds in Barchi-Kol (Korsakov et al. 2002). The non-UHP units of the Kokchetav complex are composed of metabasic rocks (eclogites and amphibolites), orthogneisses (gneisses of granitic composition, e.g. composed mainly of quartz and feldspars, and with low content of mafic minerals) and metasediments.

The protolith for the Kokchetav UHP rocks were shales with intercalated dolomite limestone and associated with minor mafic magmatic rocks (Shatsky et al. 1995, 1999, 2006). The sediments were deposited at a passive continental margin, while the mafic magmatism occurred during continental rifting (Shatsky et al. 1999). The geochemistry of eclogites from the Kokchetav complex was studied previously (Gilbert et al. 1990; Shatskiy et al. 1990). The basement rocks are represented by felsic orthogneisses, which were formed at 1,128–1,169 Ma (Letnikov et al. 2007; Turkina et al. 2011; Tretyakov et al. 2011). Turkina et al. (2011) classified the protolith of the gneisses as A-type granites and attributed them to crustal melts formed in a continental rift zone. The age of detrital zircon cores and ancient Nd model ages of the Kokchetav metasediments indicate that these granitoid rocks intruded a pre-existing continental crust (Shatsky et al. 1999). UHP metamorphism occurred at ~535–525 Ma (Claoue-Long et al. 1991; Hermann et al. 2001; Katayama et al. 2001; Ragozin et al. 2009). Subduction of the Kokchetav microcontinent continued during and after formation of the UHP complexes until the final collision, which occurred at 470–480 Ma (Hacker et al. 2003; Zhimulev et al. 2010, 2011) and was sealed by the large Zerenda batholith that intruded at 460–440 Ma (Shatagin et al. 1999, 2001).

Analytical methods

Phase relationships were determined in polished thin sections using an optical microscope and a JEOL 6400 scanning electron microscope (SEM) at the Centre for Advanced Microscopy, ANU. Back-scattered electron images (BSE) were obtained, and the major element compositions of all phases were determined by EDS using an accelerating voltage of 15 kV and a beam current of 1 nA.

For bulk rock analyses, the samples were ground in either a tungsten carbide mill or in a steel mill (Table 1) to a grain size of <400 μm. They were powdered to <25 μm in an alumina oxide mill. Loss on ignition was determined by heating 1–2 g of crushed sample at 1,050 °C for 3 h in a platinum crucible. Na, Mg, Al, Si, P, K, Ca, Ti, Mn, Fe, and S concentrations were measured by XRF of fused discs with a Phillips (PANalytical) PW2400 X-ray fluorescence spectrometer at RSES, ANU. The lithium borate fusion discs were prepared by fusion of 0.27 g of sample powder and 1.72 g of "12–22" eutectic lithium metaborate-lithium tetraborate. The major elements were calibrated against 28 international standard rock powders. Another set of

Table 1 List of samples used in this study, their mineral associations, analytical details and geochemical classification

Sample	Location	DH	Rock type	Lab	Mill	REE type	Rock forming minerals	Accessory minerals	*P* (kbar)	*T* (°C)	Ref.
B94-355	Barchi-Kol	124	Grt gneiss	ANU	SM	UD	Grt, Ky, Kfs, Phe, Qtz	Rt	>45	950–1,000	SSH, HRK
B94-57	Barchi-Kol	112	Grt-Bt gneiss	ANU	WC	SD	Grt, Kfs, Pl, Qtz, Bt	Rt, Zrn, Ap, Sulf	>45	950–1,000	SSH, HRK
B94-29	Barchi-Kol	111	Grt-Bt gneiss	ANU	WC	SD	Grt, Bt, Ky, Qtz, Kfs	Zr, Rt, Ap	>45	950–1,000	SSH, HRK
B118A50	Barchi-Kol	118	Grt-Bt gneiss	ANU	WC	SD	Grt, Kfs, Pl, Bt, Phe, Qtz	Zrn, Rt, Th min*, U min*, Mnz*, Sulf, Dia	>45	950–1,000	SSH, HRK
B94-60	Barchi-Kol	112	Grt-Bt gneiss	ANU	WC	SD	Grt, Bt, Qtz, Kfs, Pl	Zrn, Rt, Tnt, Aln, Mnz*, Sulf	>45	950–1,000	SSH, HRK
B118A1	Barchi-Kol	118	Grt-Bt gneiss	US, SA	SM	SD	Grt, Kfs, Pl, Bt, Phe, Qtz	Zrn, Rt, Sulf	>45	950–1,000	SSH, HRK
B118A2	Barchi-Kol	118	Grt-Bt gneiss	US, SA	SM	UD	Grt, Kfs, Pl, Bt, Phe, Qtz	Zrn, Rt, Sulf	>45	950–1,000	SSH, HRK
B118A3	Barchi-Kol	118	Grt-Bt gneiss	US, SA	SM	UD	Grt, Kfs, Pl, Bt, Qtz	Zrn, Rt, Sulf	>45	950–1,000	SSH, HRK
B118A5	Barchi-Kol	118	Grt-Bt gneiss	US, SA	SM	SD	Grt, Kfs, Pl, Bt, Phe, Qtz	Zrn, Rt, Ap, Sulf	>45	950–1,000	SSH, HRK
B118A7	Barchi-Kol	118	Grt-Bt gneiss	US, SA	SM	SD	Grt, Kfs, Pl, Bt, Phe, Qtz	Zrn, Rt, Sulf	>45	950–1,000	SSH, HRK
B118A14	Barchi-Kol	118	Grt-Bt gneiss	US, SA	SM	SD	Grt, Kfs, Pl, Bt, Phe, Qtz	Zrn, Rt, Sulf	>45	950–1,000	SSH, HRK
B118A17	Barchi-Kol	118	Grt-Bt gneiss	US, SA	SM	SD	Grt, Kfs, Pl, Bt, Phe, Qtz	Zrn, Rt, Sulf	>45	950–1,000	SSH, HRK
B94-256	Barchi-Kol	112	Mica schist	ANU	WC	ND	Grt, Qtz, Phe, Bt, Kfs	Rt*, Zrn, Aln, Mnz, Ap	>45	950–1,000	ST
B01-3	Barchi-Kol	outcrop	Mica schist	ANU	WC	ND	Grt, Qtz, Ky, Phe	Rt, Mnz, Ap*, Xen*, Zrn	≈24	≈710	ST
B94-333	Barchi-Kol	119	Grt-Bt gneiss	ANU	WC	ND	Grt, Bt, Phe, Ky, Qtz, Pl	Rt, Zrn, Ap, Mnz, Aln, Syn, Sulf	30–40	800–900	ST
B95-99	Barchi-Kol	121	Grt-Bt gneiss	US, SA	SM	ND	Grt, Phe, Bt, Rt, Kfs, Pl	Rt, Zrn, Ap, Mnz, Aln	20–25	≈800	ST
KY98-3	Kulet	outcrop	Cordierite fels	ANU	WC	ND	Crd, Qtz, Bt, Kfs	Ilm, Sp, Mnz	1–3	570–670	TO
CHAG	Chaglinka	Outcrop	Grt-Bt gneiss	ANU	WC	ND	Phe, Ky, Bt and Qtz.	Brt*, Mnz, Zrn	7.5–9	530	MP
G03	Sulu-Tjube	Outcrop	Mica schist	US, SA	SM	ND	Grt, Phe, Bt, Qtz, Ky	Rt, Zr, Tur, Mnz	13	620 ± 50	PYP
KY98-18	Kulet	Outcrop	Orthogneiss	ANU	WC	ND	Qtz, Kfs, Pl, Bt	Zrn, Mnz	34–36	720–760	P
KK03-1	Kumdy-Kol	Outcrop	Orthogneiss	ANU	WC	ND	Qtz, Phe, Pl, Kfs	Aln, Zrn, Ap			KV
KK03-2	Kumdy-Kol	Outcrop	Qtz-mica schist	ANU	WC	ND	Qtz, Phe	Zrn, Mnz			KV
Q03-11A	Enbek Berlyk	Outcrop	High Al gneiss	ANU	WC	ND	Cor, Ky, Grt, Qtz, Bt, Kfsp	Rt, Ap, Mnz	>12	740–780	DSSH
Q03-12	Enbek Berlyk	Outcrop	High Al gneiss	ANU	WC	ND	Ky, Grt, Bi, Qtz	Rt, Ap, Ilm, Mnz	>12	740–780	DSSH

DH—drill hole number or collection from surface. Lab—laboratory where bulk rock composition by XRF was obtained: ANU—Australian National University, Australia, US-SA—Stellenbosch University, South Africa. Mill—mills used for samples powdering: WC—tungsten carbide mill, SM—steel mill. REE type—classification according to LREE content: ND—non-LREE-depleted samples, SD—gneiss semi-depleted in LREE, and UD—ultra-depleted gneiss. Mineral abbreviations are according to Kretz (1983) and additionally: Dia—diamond, Sulf—sulphides, Th min—Th minerals, U min—U minerals. *—minerals which are present only as inclusions or inferred from reaction textures. References for estimates of PT conditions: SSH—–Sobolev and Shatsky (1990), HRK—Hermann et al. (2001), DSSH—Dobretsov et al. (1995), KV—Kushev and Vinogradov (1978), ST—Stepanov (2012), PYP—Perchuk et al. (1998), MP—Maruyama and Parkinson (2000), TO—Terabayashi et al. (2002) and *P*—Parkinson (2000). Coordinates: Barchi-Kol: 53.161799, 68.704705; Kumdy-Kol: 53.138843°, 68.958475°; Kulet: 53.011693°, 69.517361°; Chaglinka: 53.133052°, 69.061808°; Sulu-Tjube: 53.079506, 69.190408°; Enbek Berlyk: 53.068307°, 69.345570°

samples was measured by Axios from PANalytical with a 2.4 kW Rh X-ray Tube in the Central Analytical Facility of Stellenbosch University, South Africa. One gram of sample powder was mixed with 10 g of Claisse flux and fused in M4 Claisse fluxer for 23 min.

Trace elements were analysed by LA-ICP-MS of fused discs with 1:3 sample/lithium borate ratio at RSES, ANU, using a pulsed 193 nm ArF Excimer laser with 100 mJ energy at a repetition rate of 5 Hz (Eggins et al. 1998), coupled to an Agilent 7500 quadrupole ICP-MS. Laser sampling was performed in a He–Ar–H_2 atmosphere using a spot size of 105–137 μm in different parts of the lithium borate fused discs. Data acquisition was performed by peak hopping in pulse counting mode, acquiring individual intensity data for each element during each mass spectrometer sweep. A total of 60 s, comprising a gas background of 20–25 s, was performed for each analysis. The LA-ICP-MS data were processed by an in-house Excel spreadsheet created by Charlotte Allen. Compositions were calculated using NIST 612 glass as external standard with the reference values reported by Jochum (2011) and SiO_2 from XRF data as the internal standard. The resulting data are the average of 4–5 ablation spots; one standard deviation from the average is <5 % relative for most elements. BCR–2 glass was measured as secondary standard, and deviation from values by Norman et al. (1998) was <5 % for all elements.

Sample description

Main minerals and textures

This study aims to determine the effect of UHP melting on the composition of metasedimentary rocks of the Kokchetav complex. Therefore, two types of samples were selected from our large collection of rocks: (a) non-UHP schists and gneisses from various localities of the Kokchetav complex (Fig. 1) and (b) drill core samples of garnet-bearing gneisses and schists from the Barchi-Kol UHP terrain, representing the dominant UHP rock type in the Kokchetav complex. A summary of rock forming minerals, accessory phases as well as estimated P–T conditions of all the analysed samples is given in Table 1. Mineral abbreviations are according to Kretz (1983).

The samples of non-UHP rocks originate from several localities of the Kokchetav complex and were selected in order to obtain a representative spectrum of metasedimentary and felsic rocks in the Kokchetav metamorphic belt (Fig. 1). These rocks cover a wide range of metamorphic conditions (Table 1). Sample KK03-1 is an orthogneiss, which was taken from an outcrop on the shore of lake Kumdy-Kol to the east of the entrance of the Kumdy-Kol exploration gallery, from a sequence of gneisses and mica schists with lenses of eclogites (Kushev and Vinogradov 1978). Sample KK03-2 is from the same outcrop as KK03-1 and is composed mainly of quartz and phengitic mica. Sample CHAG is a mica schist sampled in outcrop at the bank of the Chaglinka river. The rock contains large garnet porphyroblasts (>10 mm) partially replaced by biotite and surrounded by a matrix of quartz, kyanite, phengite and biotite. Samples Q03-11A and Q03-12 are "metaconglomerate" gneisses with grey nodules embedded in a dark matrix from an outcrop in the Enbek-Berlyk area. They contain characteristic grey ovoids, which are composed of kyanite and minor corundum. The ovoids are surrounded by coronas of biotite, garnet and feldspars. Sample G03 is a mica schist from the Sulu-Tjube area composed of garnet, phengite, biotite, quartz and kyanite. The rock is strongly foliated and contains coarse phengite porphyroblasts and large tourmaline grains aligned along the foliation. Sample Ky98-18 is an orthogneiss from the outcrop near the Kulet UHP terrain, located within 100 m of the outcrop with UHP whiteschists (Parkinson 2000). The orthogneiss experienced deformation evident from small isoclinal folds. Ky98-3 is a cordierite hornfels from the Daulet suite outcrop in the Kulet area. The rock has a massive texture and is composed mainly of cordierite and quartz with minor biotite, K-feldspar and spinel.

Samples from the Barchi-Kol area were selected from the collection of drill core material obtained by the Kokchetav Prospecting Expedition. Most of the samples are fresh, as is evident from the presence of non-oxidized sulphides. The garnet-biotite gneisses are composed of fine-grained Grt, Kfs, Pl, Bt, Phe and Qtz (Fig. 2). Accessory minerals are Zrn, sulphides, ±Rt, ±Ttn, ±Ap and sometimes REE minerals. Textures of the gneisses are variable and range from highly foliated rocks with layers of different mineralogy (e.g. B94-60 and B94-29, Fig. 2) to weakly foliated rocks (e.g. B94-57 and B118A2, B118A50, Fig. 2) where the foliation is defined by alternating layers enriched in micas or quartz and feldspar. In most gneisses biotite, phengite and rutile have a preferred orientation. Feldspars grains are isometric and lack systematic orientation. In the majority of samples, garnet crystals are small (1–3 mm), fractured and commonly have biotite rims. Sample B94-355 differs from other samples by the presence of kyanite, which forms resorbed grains in the matrix, and the low abundance of biotite. The texture of the majority of Barchi-Kol samples is gneissic with variable extent of segregation of quartz–feldspar-rich material on a millimetre scale (Fig. 2), resembling migmatites (Sawyer 2008). These segregations merge occasionally into slightly discordant veins (e.g. B94-60, Fig. 2), suggesting that the gneisses experienced partial melting. The samples from UHP terrains display a variable degree of retrogression,

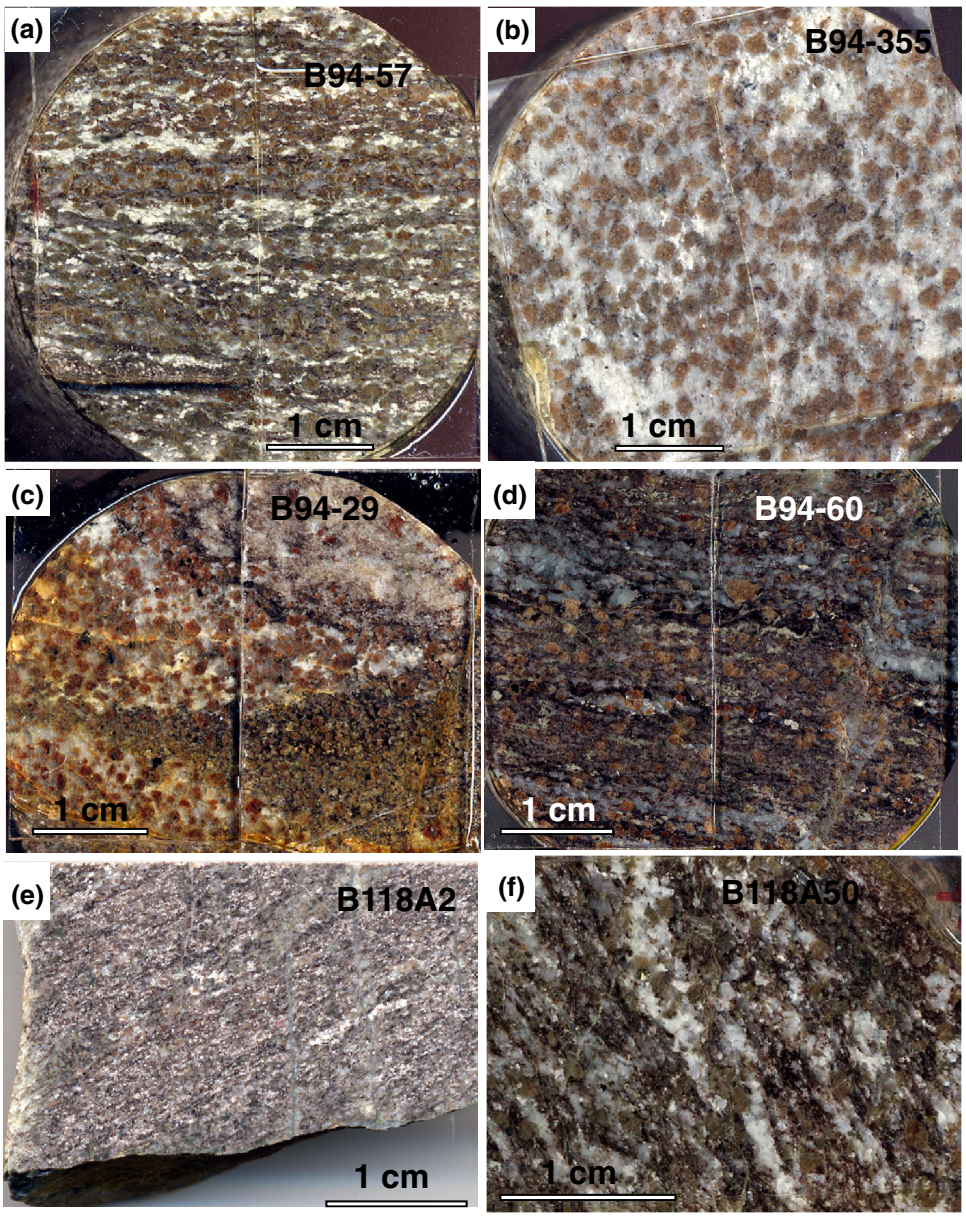

Fig. 2 Scanned images of polished rock slabs of UHP gneisses. The rocks are rich in garnet and show gneissic texture: *dark areas* are mostly composed of garnet and biotite, whereas light coloured bands are enriched in feldspars and quartz

which is represented by sericitization of feldspars, chloritization of micas and elevated LOI. Shatsky et al. (1999) demonstrated that this low temperature retrogression did not produce a significant alteration of the composition of UHP gneisses. Samples B118A1-B118A17 were collected from a depth of 58–61 m of the drill hole 118 in the Barchi-Kol unit, which contained numerous diamond-bearing rocks. These 8 samples represent the metre scale heterogeneity of the UHP gneisses. Despite rare occurrence of diamonds in our samples (diamonds observed only in sample B118A50), we are confident that they all experienced UHP metamorphism because of their close metre scale association with diamond-bearing rocks. This is further supported by the unusual geochemistry of the garnet-biotite gneisses, which is the main topic of this study.

Four samples from the Barchi-Kol UHP area (B01-3, B94-333, B94-256 and B95-99) have distinct compositional and textural features compared to the diamond-bearing gneisses (Stepanov 2012). Samples B01-3 and B94-256 are foliated mica schists with large amounts of white mica that do not show any macroscopic evidence for partial melting. In B01-3, phengite occurs as large euhedral flakes. Grains of kyanite are small and often have an irregular, resorbed shape and are enclosed in phengite. Garnet crystals are euhedral and have a bimodal distribution with large crystals of >3 mm and small grains <0.5 mm. In B94-256, garnet and phengite crystals are homogeneously distributed thought the rock. Biotite occurs as small grains along the edges of phengite and garnet and has random orientation. Zircon and monazite form coarse

grains, and monazite occasionally has a corona of apatite. Rutile is present only as inclusions in garnet and is absent in the matrix. B94-333 has a gneissic texture with layers with substantially different mineralogy and mineral compositions. One such layer contains abundant grains of rounded kyanite, whereas in other parts of the sample kyanite is absent. Another layer contains large grains of elongated pink garnet (>5 mm) that have pressure shadows. B95-99 is a mica schist cut by a leucogranite vein, with large phengite and garnet crystals adjacent to the vein. B94-333 and B95-99 show some textural evidences of melting (gneissose texture and veins of Qtz-Fsp-Phe aggregate in sample B95-99), but they experienced lower peak metamorphic conditions than the UHP gneisses (Stepanov 2012).

REE minerals in the Kokchetav metasediments

In order to understand the behaviours of LREE, Th and U during UHP metamorphism, we have conducted a systematic investigation of accessory minerals using BSE imaging and mineral analysis. We compared which accessory minerals host these elements in UHP gneisses and non-UHP samples.

In the majority of non-UHP samples, the dominant LREE phase is monazite (Table 1), which usually forms well-developed large grains 100–200 μm in size (Fig. 3a, b). Allanite is the main LREE phase in sample KK03-1. In sample CHAG, kyanite and garnet contain polyphase inclusions of monazite and apatite likely replacing bearthite $(Ca,REE)_2Al(PO_4)_2(OH)$, a REE-rich phase that has been found also in other UHP rocks (Chopin et al. 1993; Scherrer et al. 2001). Similarly, in sample Q03-12, monazite is present either as separate grains or in aggregates of apatite and monazite. It is likely that monazite in these associations also was formed from breakdown of bearthite.

The four samples from Barchi-Kol (B01-3, B94-333, B94-256 and B95-99) with limited macroscopic and geochemical evidence for melting contain abundant LREE, Th and U minerals. A rich association of REE minerals was observed in sample B94-333 (Fig. 3c, d). It contains monazite inclusions in garnet and matrix, and several reactions involving REE-bearing minerals can be observed. One monazite grain is located between garnet and an apatite crystal with inclusions of Th-orthosilicate minerals. In the matrix, there are grains of allanite and a relatively rare mineral synchysyte $(La,Ce)Ca(CO_3)_2F$ with low Th content. In B95-99, monazite is partly replaced by allanite.

In the majority of UHP gneisses LREE, Th and U minerals are rare. Sample B118A50 contains an aggregate of high-pressure phengite, huttonite ($ThSiO_4$) and phosphates with variable compositions (Fig. 3g–j). Morphology and composition of this aggregate suggest that this is an allanite pseudomorph. This rock also contains large rutile grains with inclusions of uraninite (Fig. 3j). Rutile is surrounded by a symplectite of Rt-Phe with Nd-rich monazite (Fig. 3i). In B94-60, allanite grains are present in the matrix (Fig. 3g, h) and a large titanite grain has been partly replaced by a symplectite of rutile with phengite, containing small monazite grains. In other samples from Barchi-Kol, we did not find LREE minerals, in line with the low concentration of LREE in these depleted gneisses.

Results

Major elements

Major element variation diagrams of the analysed samples and samples reported by Shatsky et al. (1999) and Buslov and Vovna (2008) are presented in Fig. 4. The rocks from the non-UHP terrains form several distinct groups: orthogneisses have high SiO_2, $Na_2O + K_2O$ and low FeO and MgO (Fig. 4); sandstones from the study by Buslov and Vovna (2008) have the highest SiO_2 and lowest FeO and MgO; and terrigenous metasediments (represented by schists and gneisses) have high FeO, MgO and Al_2O_3 but also moderately high $Na_2O + K_2O$. Phengite-rich sample KK03-2 has a similar major element composition as the orthogneisses, and thus, it is interpreted as an altered, hydrated granite.

UHP gneisses show SiO_2 contents similar to non-UHP terrigenous metasediments from this study (Table 2), lower Al_2O_3 and K_2O concentration, whereas CaO, Na_2O, FeO and MgO are commonly higher in the UHP than the non-UHP samples (Fig. 4). K_2O and FeO + MgO in UHP gneisses are negatively correlated, whereas in non-UHP metasediments, these parameters are scattered and are not correlated (Fig. 4). Samples of UHP gneisses from this study and UHP samples from Shatsky et al. (1999) with CaO >6 % overlap in all major oxides. Samples from Buslov and Vovna (2008) have SiO_2 and K_2O similar to non-UHP gneisses and schists, but their Al_2O_3, Na_2O and CaO contents are higher than in non-UHP metasediments and are comparable to gneisses from Barchi-Kol reported in this study (Fig. 4).

Lanthanides and actinides: REE, Th and U

The non-UHP samples from this study (Table 2) have chondrite-normalized patterns typical for crustal rocks (Taylor and McLennan 1985) with a decrease from La to Sm–Tb, flat HREE and a negative Eu anomaly (Fig. 5). The non-UHP terrigenous metasediments from the study of Shatsky et al. (1999) and our study have a high LREE

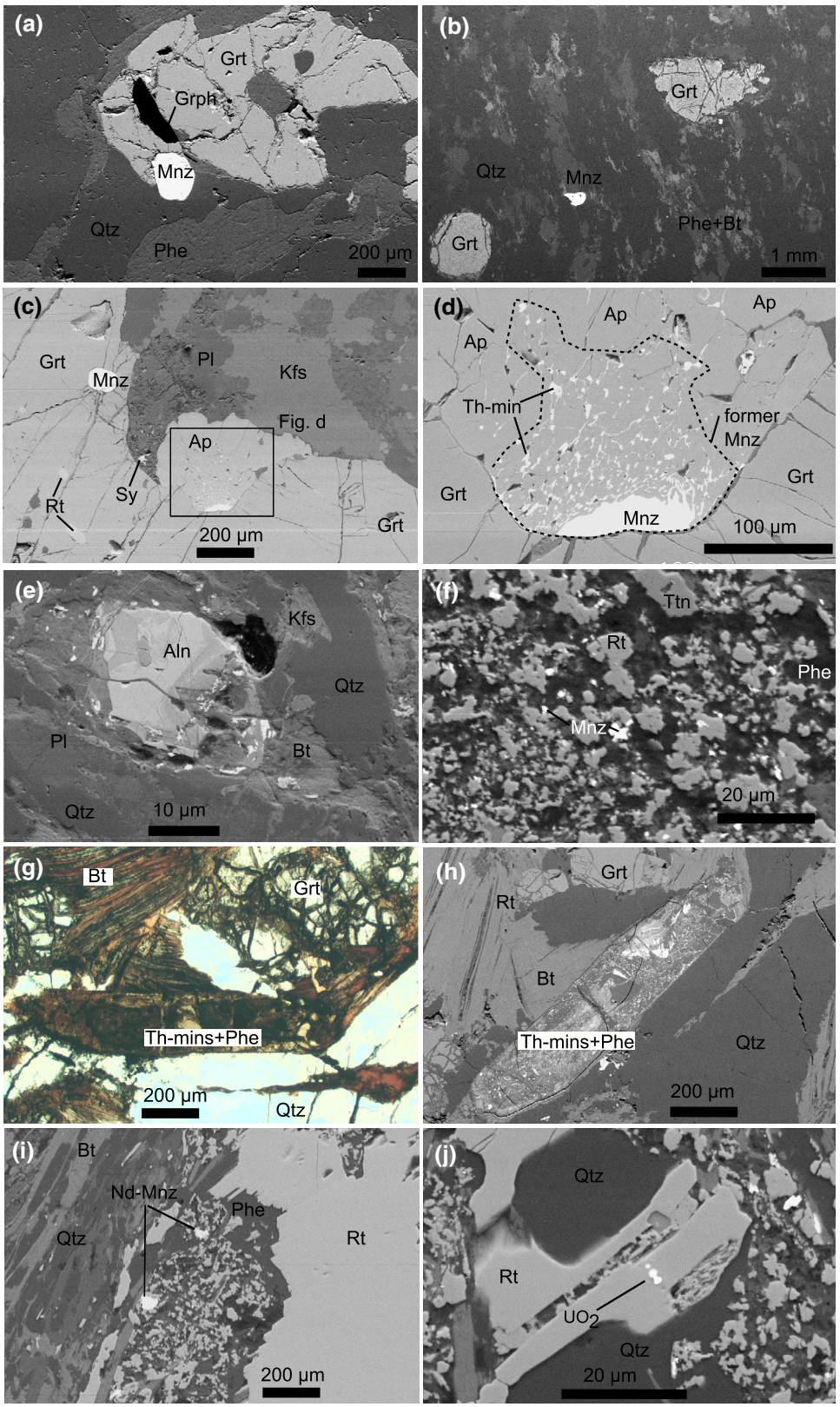

Fig. 3 Textures of LREE minerals in Kokchetav samples without LREE depletion (**a–d**) and in LREE-depleted samples (**e–j**). **a** Sample B01-3 and **b** sample B96-256 contain coarse monazite grains; **c–d** sample B94-333 shows textures of monazite replacement; **e–f** sample B94-60 with large allanite grains and minor monazite; **g–j** sample B118A50 with complex association of LREE–Th–U minerals. *Mnz* monazite, *Aln* allanite, *Sy* synchysyte (La,Ce)Ca$(CO_3)_2$F, other mineral abbreviations according to Kretz (1983)

content (20–80 La ppm) accompanied by high Th (8–30 ppm). Orthogneisses show large variations in REE contents and sub-parallel patterns.

The REE compositions of gneisses from Barchi-Kol are highly variable, ranging from high–LREE patterns in non-UHP rocks (B94-256, B95-99, B01-3, B94-333) to patterns

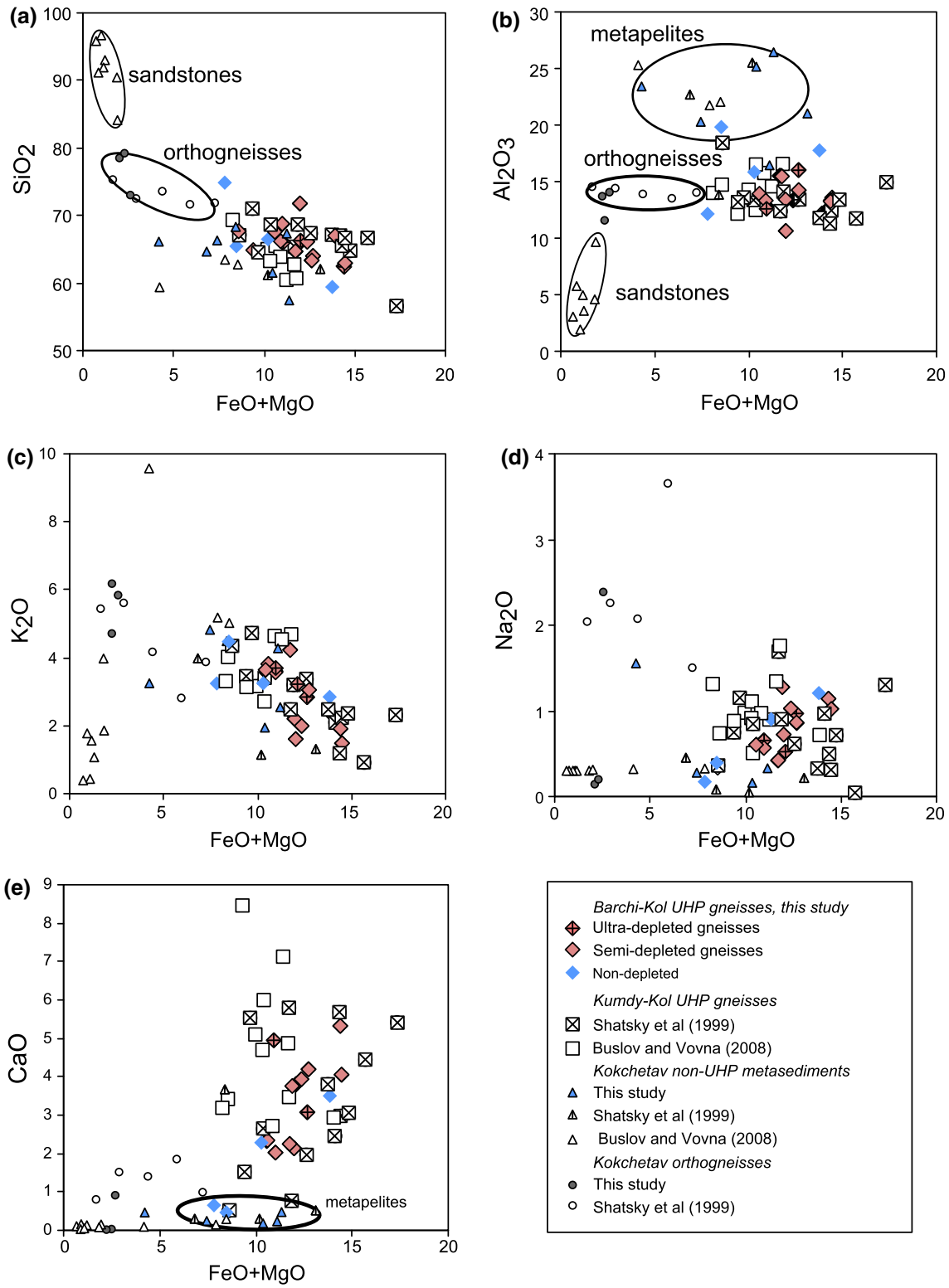

Fig. 4 Major element compositions of non-UHP metasediments and orthogneisses, and UHP gneisses from Barchi-Kol, and Kumdy-Kol terrains from the published studies and this work

with strong depletion in LREE relative to HREE (Fig. 5). Some gneisses have patterns with lower Pr and Nd relative to La and Sm, but generally patterns are flat at 10–30 times chondrite. Irrespective of LREE content, Barchi-Kol gneisses have a similar Eu anomaly Eu/Eu* = 0.50–0.77, which is similar to the Eu anomaly of non-UHP

Table 2 Major and trace element compositions of the gneisses from the Kokchetav complex

Sample	B94-355	B94-57	B94-29	B118 A50	B94-60	B118 A1	B118 A2	B118 A3	B118 A5	B118 A7	B118 A14	B118 A17
Type	UD	SD	SD	SD	SD	SD	UD	UD	SD	SD	SD	SD
SiO_2	62.3	59.0	70.8	63.0	60.2	62.3	63.9	64.4	65.9	65.1	63.1	60.3
TiO_2	0.92	1.74	0.62	0.65	0.95	0.75	0.54	0.44	0.55	0.60	0.63	0.63
Al_2O_3	15.7	12.7	10.4	12.8	12.8	14.9	12.4	13.1	12.7	13.3	12.7	13.4
Fe_2O_3	9.2	11.2	10.2	7.9	9.1	8.4	6.4	7.6	7.3	6.8	8.0	7.7
MnO	0.15	0.32	0.40	0.37	0.24	0.19	0.23	0.23	0.21	0.21	0.37	0.26
MgO	4.2	3.5	2.6	4.3	5.6	3.7	4.9	4.9	3.9	4.0	4.6	5.0
CaO	3.0	3.8	2.1	3.6	5.1	2.2	4.8	3.7	2.0	2.2	3.7	4.0
Na_2O	0.96	0.96	0.71	1.22	1.10	0.41	0.64	0.50	0.55	0.59	0.97	0.81
K_2O	2.8	1.4	1.6	2.1	1.8	4.1	3.6	3.1	3.4	3.6	1.9	2.9
P_2O_5	0.04	0.23	0.03	0.11	0.15	0.12	0.02	0.03	0.07	0.07	0.08	0.08
SO_3	0.16	0.88	bdl	0.53	0.16	na	na	na	na	na	na	na
LOI	0.33	4.86	0.24	3.86	3.41	3.26	2.02	1.37	2.36	3.44	3.98	4.74
Total	99.5	95.6	99.5	96.5	97.4	97.0	97.3	98.1	96.7	96.6	96.0	95.1
Be	bdl	2.1	0.7	1.9	2.5	0.93	2.0	1.9	1.6	1.4	2.3	2.9
Sc	26	31	24	18	25	21	15	16	18	16	20	25
Cr	108	40	248	73	186	92	56	53	69	63	73	193
Co	25	33	19	26	27	24	19	23	22	21	17	23
Ni	53	45	65	36	57	39	25	30	51	26	37	42
Cu	26	57	3	85	42	126	12	151	143	18	55	8.2
Zn	47	129	152	109	100	88	47	44	87	76	110	112
As	1.6	10.1	5.7	1.4	5.2	1.4	0.7	0.9	1.1	1.8	1.3	1.3
Rb	91	79	63	115	104	197	177	157	200	188	109	156
Sr	71	51	45	36	47	18	41	22	23	22	35	37
Y	40	49	28	32	30	32	21	24	28	27	35	22
Zr	77	209	166	155	182	187	221	150	165	179	190	164
Nb	14	17	12	7.4	9.3	14	9.9	5.7	6.6	10.8	8.5	5.5
Mo	1.9	3.7	1.5	1.5	1.4	3.5	0.9	1.8	2.5	1.4	1.4	1.4
Sb	3.1	4.8	3.9	3.6	3.7	na	na	na	na	na	na	na
Cs	0.9	4.3	1.1	3.9	6.2	3.8	4.2	3.5	5.2	3.9	4.0	6.7
Ba	99	65	150	77	111	145	72	56	89	147	70	108
La	2.2	7.9	4.1	10	10	6.5	1.0	0.4	11.3	6.4	10.5	12
Ce	2.7	16	6.8	21	24	17.1	2.5	0.9	27	15	20.1	22
Pr	0.3	2.2	0.8	2.5	3.2	2.1	0.4	0.1	3.3	1.7	2.5	2.4
Nd	1.5	10	3.3	11	15	9.4	1.8	0.8	14	7.2	11	10
Sm	1.3	3.7	1.5	3.4	4.0	3.0	0.8	0.5	3.1	2.1	3.8	2.4
Eu	0.5	1.0	0.4	0.8	0.8	0.8	0.3	0.2	0.5	0.6	0.9	0.6
Gd	3.6	5.8	2.4	4.5	4.7	4.4	1.6	1.6	3.4	3.4	5.3	3.1
Tb	0.8	1.1	0.5	0.8	0.8	0.8	0.3	0.4	0.7	0.7	0.9	0.6
Dy	6.7	8.2	4.2	5.6	5.4	5.5	3.0	3.8	4.7	4.8	6.3	3.9
Ho	1.5	1.8	1.0	1.2	1.1	1.2	0.8	0.9	1.0	1.0	1.3	0.8
Er	4.6	5.6	3.3	3.4	3.3	3.6	2.6	3.0	3.3	3.2	3.8	2.6
Tm	0.7	0.8	0.5	0.5	0.5	0.5	0.4	0.5	0.5	0.5	0.5	0.4
Yb	4.9	5.6	3.6	3.4	3.3	3.5	3.0	3.3	3.4	3.2	3.7	2.5
Lu	0.7	0.8	0.6	0.5	0.5	0.5	0.5	0.5	0.5	0.5	0.5	0.4
Hf	2.1	5.9	4.7	4.5	5.2	5.6	6.8	4.6	4.7	5.5	5.5	4.8
Ta	0.6	1.9	2.1	1.0	1.3	0.9	0.5	0.3	0.4	1.1	1.0	0.3
Pb	2.6	4.4	4.7	1.9	4.5	1.5	0.5	0.7	4.5	0.8	1.4	2.0
Th	0.3	2.4	1.6	4.1	4.3	1.7	0.0	0.1	2.2	3.8	5.0	4.3
U	0.7	18.8	0.6	1.5	2.6	0.5	0.3	0.2	0.7	0.7	2.1	1.0

Table 2 continued

Sample	B94-256	B01-3	B94-333	B95-99	KY98-3	CHAG	G03	KY98-18	KK03-1	KK03-2	Q03-11A	Q03-12
Type	ND	ND	ND	ND	ND	ND	ND	ND	ND	ND	ND	ND
SiO_2	73.1	63.7	56.6	64.2	64.6	64.0	63.1	77.5	61.7	76.6	59.1	54.1
TiO_2	0.81	0.79	1.23	0.74	0.92	0.81	0.60	0.22	0.36	0.23	1.02	0.87
Al_2O_3	11.8	19.3	17.0	15.3	15.9	22.7	19.4	11.4	11.8	13.5	24.3	24.9
Fe_2O_3	6.0	7.7	10.1	8.1	8.4	3.6	6.6	2.4	1.9	2.2	6.5	8.5
MnO	0.25	0.12	0.16	0.14	0.17	0.08	0.17	0.004	0.004	0.01	0.04	0.08
MgO	2.3	1.4	4.1	2.7	3.3	0.9	1.2	0.2	0.5	0.2	4.2	3.1
CaO	0.6	0.4	3.3	2.2	0.2	0.4	0.2	0.04	0.8	0.0	0.1	0.4
Na_2O	0.16	0.38	1.14	0.88	0.32	1.50	0.25	0.20	2.03	0.14	0.15	0.84
K_2O	3.2	4.3	2.7	3.1	4.1	3.1	4.6	6.0	4.9	4.6	1.9	2.4
P_2O_5	0.06	0.04	0.21	0.04	0.08	0.16	0.06	0.07	0.24	0.02	0.07	0.07
SO_3	bdl	bdl	0.08	na	bdl	bdl	na	bdl	bdl	bdl	bdl	bdl
LOI	1.44	1.73	2.16	3.56	2.50	1.77	3.9	1.65	1.75	0.14	3.82	2.15
Total	98.3	98.3	96.9	97.3	98.1	97.3	96.1	97.9	84.3	97.4	97.3	95.3
Be	1.7	2.6	2.1	2.3	1.8	3.6	3.0	2.9	1.9	3.3	1.8	5.4
Sc	17	19	29	24	19	21	17	12	9	12	13	12
Cr	97	95	97	201	78	112	203	8.7	11	8.4	150	160
Co	31	19	26	21	22	15	17	7.2	15	4.9	22	20
Ni	47	30	37	47	33	25	26	4.0	8.4	6.0	46	41
Cu	27	19	14	44	23	12	40	4.9	4.5	2.1	10	33
Zn	66	27	52	42	62	35	36	47	5.3	49	50	70
As	1.5	2.1	4.6	8.6	1.1	2.7	1.2	1.2	1.3	0.8	3.6	2.4
Rb	125	187	137	180	103	144	167	223	140	231	74	103
Sr	6.7	26	51	43	21	95	43	23	81	11	13	75
Y	34	41	42	39	25	47	23	34	28	35	27	22
Zr	312	202	219	228	140	232	145	357	188	325	232	196
Nb	12.9	20.1	25.1	14.6	10.5	21.3	15.3	17.0	21.2	19.3	14.9	16.2
Mo	2.5	1.2	1.2	2.0	0.7	1.1	1.9	0.7	0.6	0.6	0.8	0.8
Sb	3.4	3.1	3.2	na	2.4	3.1	na	3.3	2.5	3.2	3.1	3.0
Cs	2.4	4.1	2.7	4.2	8.4	3.3	2.3	4.5	1.3	6.1	3.9	4.4
Ba	238	535	295	317	422	557	639	1,053	772	619	211	652
La	25	68	60	31	26	65	31	63	58	33	69	87
Ce	51	137	120	62	55	127	71	127	123	64	138	168
Pr	5.8	15	14	7.0	6.2	14	7.0	14	12	7.3	15	19
Nd	23	55	53	27	25	54	26	52	45	28	59	71
Sm	4.2	9.8	10.8	6.2	4.8	10.1	4.9	9.3	8.2	5.2	10.2	11.5
Eu	0.8	1.6	1.8	1.2	1.0	1.9	1.0	1.2	1.0	0.6	0.7	1.9
Gd	4.2	8.2	9.3	6.6	4.5	9.6	4.1	7.7	6.5	4.5	7.9	8.3
Tb	0.7	1.3	1.3	1.1	0.7	1.4	0.7	1.1	0.9	0.8	1.0	1.0
Dy	5.2	8.2	8.2	7.3	4.3	8.8	4.5	6.5	5.6	5.5	5.6	5.0
Ho	1.2	1.6	1.6	1.4	0.9	1.7	0.9	1.3	1.0	1.2	1.0	0.8
Er	3.6	4.6	4.5	4.3	2.6	4.9	2.7	4.0	3.0	4.1	2.8	2.1
Tm	0.5	0.7	0.6	0.6	0.4	0.7	0.4	0.6	0.4	0.7	0.4	0.3
Yb	3.5	4.6	4.3	4.0	2.6	4.8	2.6	4.2	2.9	4.6	2.7	1.8
Lu	0.5	0.7	0.6	0.6	0.4	0.7	0.4	0.7	0.4	0.7	0.4	0.3
Hf	8.4	5.8	5.9	6.7	3.9	6.7	4.2	9.6	5.5	9.1	6.4	5.4
Ta	1.4	2.1	2.8	1.3	1.1	2.2	1.4	1.8	1.9	1.8	1.4	1.5
Pb	1.2	4	5.1	5.1	10	15	6.2	14	7	8	3	10
Th	7.6	28	26	18	9	26	20	29	31	28	22	27
U	1.4	4.6	4.8	3.8	2.2	6.4	2.4	3.2	3.8	2.3	2.6	2.5

bdl below detection limit, *na* not analysed. Type is same classification according LREE content as in Table 1

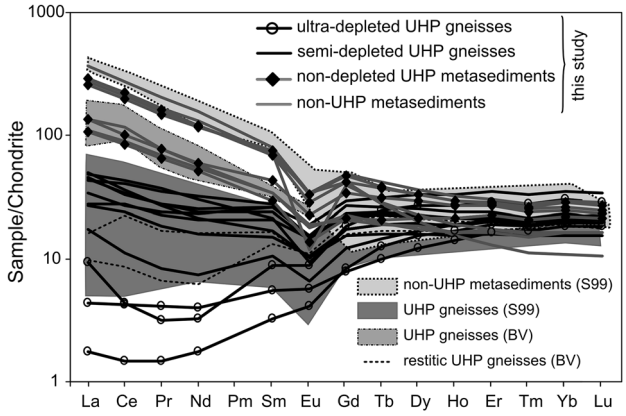

Fig. 5 Chondrite (McDonough and Sun 1995) normalized REE patterns of non-UHP metasediments compared with various types of UHP gneisses from Barchi-Kol (this study) and from Kumdy-Kol (Shatsky et al. 1999 (S99); Buslov and Vovna 2008 (BV))

metasediments and the typical value of post-Archean sediments (Taylor and McLennan 1985; Condie 1993).

The majority of samples from Barchi-Kol in our study and the garnet-bearing gneisses from Kumdy-Kol (Shatsky et al. 1999) show much lower LREE than the non-UHP samples. REE from La to Nd are strongly depleted, Sm to Dy are moderately depleted or have contents similar to the non-UHP samples and from Ho to Lu concentrations show a similar range in both groups (Fig. 5). Since the variation in LREE is the most distinct feature of the studied samples, we have subdivided the gneisses from Barchi-Kol into three groups according to their LREE content: *ultra-depleted* samples with La <6 ppm, *semi-depleted* samples with $6 < La < 12$ ppm and samples *without LREE depletion* with La >20 ppm. In the following, we will use this classification to describe other chemical characteristics of the studied rocks. The relation between rock type and REE characterization is given in Table 1. Most of the samples from Barchi-Kol in this study and all Kumdy-Kol gneisses from Shatsky et al. (1999) display variable degrees of LREE depletion. In contrast, the majority of UHP gneisses reported by Buslov and Vovna (2008) have undepleted LREE contents, with the exception of two samples that are also depleted (Fig. 5). The variable shape of REE patterns of gneisses from the Barchi-Kol and Kumdy-Kol UHP terrains is also reflected in the variation of ratios like La/Sm, Yb/Sm and Sm/Nd. On the contrary, the Sm/Nd of the non-UHP samples (Table 2) are confined at 0.17–0.24 and close to the value of 0.17 of the average continental crust (Taylor and McLennan 1985) and 0.21 in GLOSS (Global Oceanic Subducted Sediments, Plank and Langmuir 1998). In the LREE-depleted gneisses, Sm/Nd is always higher from 0.23 to 0.86, with the ultra-depleted samples and sample B94-29 having Sm/Nd >0.4.

Th and U concentrations in the LREE-depleted gneisses are much lower than in the non-UHP samples, and Th/U is remarkably variable from 0.14 to 6 (Table 2). The ultra-depleted samples have low Th/U of 0.14–0.46, while the semi-depleted samples have Th/U from 2.5 to 6, overlapping with Th/U of 4–8 in non-UHP samples. Sample B94-57 from Barchi-Kol has a higher U content of 18 ppm. Such an anomalous high U content requires confirmation and thus will not be discussed below.

Large ion lithophile elements: K, Rb, Cs, Sr, Ba and Pb

Concentrations of Rb, Cs and Sr are variable and mostly overlapping in UHP and non-UHP Kokchetav samples from this study (Fig. 6). The Rb/Sr varies widely, both in LREE-depleted Barchi-Kol gneisses (from 1.4 to 10.8) and in the non-UHP samples (1.4–5.7). All samples including UHP gneisses show a good correlation between Rb and K.

In the non-UHP metasediments, Ba concentrations range from 240 to 640 ppm, whereas in the LREE-depleted gneisses from this study, Ba is 50–210 ppm with an average of 100 ppm indicating a decrease in Ba concentrations in Kokchetav metasediments during UHP metamorphism (Fig. 7). The Pb content in the LREE-depleted gneisses (0.5–4.7 ppm) is generally lower than in non-UHP samples (1.2–14.5 ppm) and the average Pb content of 2.5 ppm in the LREE-depleted Barchi-Kol gneisses is significantly lower than 7 ppm in non-UHP metasediments.

High field strength elements: Nb, Ta, Zr, Hf and P

Nb and Ta contents in LREE-depleted gneisses are generally lower than in the non-UHP samples from this study (Fig. 6). Nb/Ta in non-UHP metasediments (Table 2) shows a narrow range of 9.6–12.6 with an average of 10.8 that is close to estimates for the continental crust composition (Fig. 7). In contrast, the LREE-depleted gneisses from Barchi-Kol (Table 2) show a large variation in Nb/Ta from 6.2 to 24. The ultra-depleted UHP gneisses from Barchi-Kol show high Nb/Ta of 21–24, with the exception of sample B94-29 that has Nb/Ta of 6.2. There is no clear correlation of Nb/Ta with LREE (Fig. 7) or K contents.

Most of the UHP gneisses investigated contain 150–230 ppm Zr, which is within the range of Zr contents in non-UHP samples (145–375 ppm, Fig. 6) and close to Zr content in GLOSS and Upper Continental Crust (UCC, Taylor and McLennan 1985). The only exception is sample B94-355, which has 80 ppm Zr. The Zr/Hf of the LREE-depleted gneisses is 34.4 ± 1, which is indistinguishable

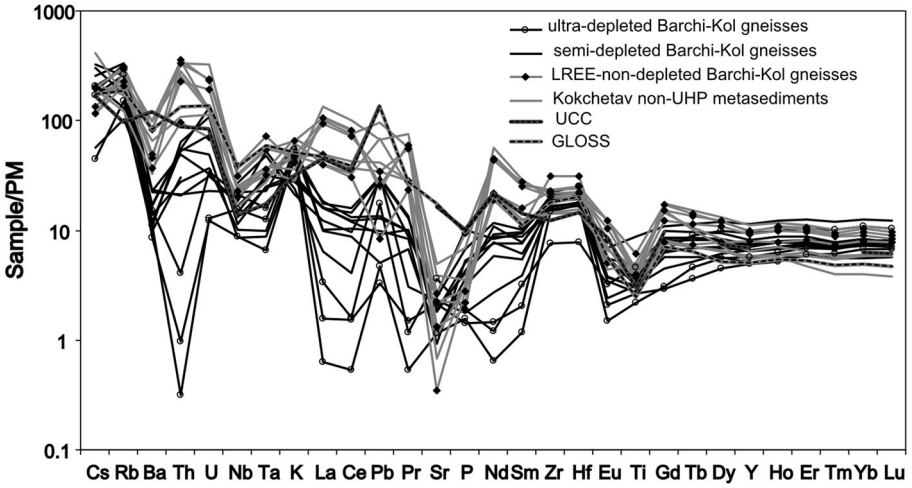

Fig. 6 Primitive mantle (McDonough and Sun 1995) normalized patterns of UHP gneisses and Kokchetav non-UHP metasediments from this study in comparison with GLOSS (Plank and Langmuir 1998) and UCC (Taylor and McLennan 1985)

from the 35 ± 1 in the non-UHP samples. There is also no correlation of Zr with FeO + MgO.

The phosphorus content of the non-UHP metasediments from studies by Shatsky et al. (1999), Buslov and Vovna (2008) and this study ranges from 230 to 1,000 ppm, with the majority of samples containing 230–400 ppm. This content is significantly lower than the average of 1,900 ppm P in modern oceanic sediments (Plank and Langmuir 1998) and 750 ppm in Proterozoic cratonic shales (Condie 1993), indicating that the Kokchetav metasediments probably had a low P content originally. In the UHP gneisses from Barchi-Kol (Table 2), the average P content is 370 ppm and a significant number of samples have lower P content than non-UHP samples. UHP gneisses from Buslov and Vovna (2008) demonstrate higher P content than the majority of LREE-depleted samples from Shatsky et al. (1999) and this study. The lowest P content of around 100 ppm is observed in the gneisses with lowest content of LREE (Fig. 7).

Discussion

Host minerals for REE, Th, U in UHP rocks

One of the key chemical features in the studied UHP gneisses is the depletion in LREE and Th. Therefore, it is important to identify what phases hosted REE, Th and U in these rocks during UHP metamorphism and exhumation. In crustal granulites, 70–95 % of LREE, Th and U are usually concentrated in accessory phases and the main hosts for LREE and Th are monazite, allanite and sometimes other rare accessory minerals (Bea 1996). However, when melting starts, accessory minerals can be dissolved in the melt, which then becomes the main host for LREE, Th and U.

In the majority of the Kokchetav non-UHP samples, LREE are concentrated in monazite (Table 1). In the UHP gneisses without LREE depletion, relatively large grains of monazite are present. In several of the LREE-depleted gneisses, complex associations of small LREE minerals were identified. Samples B94-60 and B118A50 have contained allanite as a high-pressure LREE phase (Fig. 3e, g). During retrogression, allanite decomposed and the Th and LREE were decoupled and formed Th-orthosilicate and monazite, respectively (Fig. 3e–j). In some samples, the LREE-bearing minerals were redistributed on the thin section scale and formed secondary low-Th monazite associated with Ti minerals (rutile and titanite in samples B118A50 and B94-60, respectively). We conclude that the main host for LREE, Th and U in low-grade samples was monazite and sometimes allanite, whereas in the UHP gneisses LREE, Th and U are stored in retrograde minerals such as monazite, Th-orthosilicate, U minerals and synchysyte.

Evidence for partial melting and melt extraction

The Kokchetav gneisses display many macroscopic features of migmatites (Fig. 2) indicating that at some stage in their metamorphic evolution, they experienced a partial melting event (Sawyer 2008). In this section, we compare the observed major and trace element composition of the gneisses with melting trends observed in partial melting experiments to better constrain the extent and conditions of partial melting.

Numerous experimental studies have demonstrated that melting of metapelites and metagraywackes produces peraluminous granitic melts of broadly similar haplogranitic composition over a large range of P–T conditions from crustal to subduction zone environments (Vielzeuf and

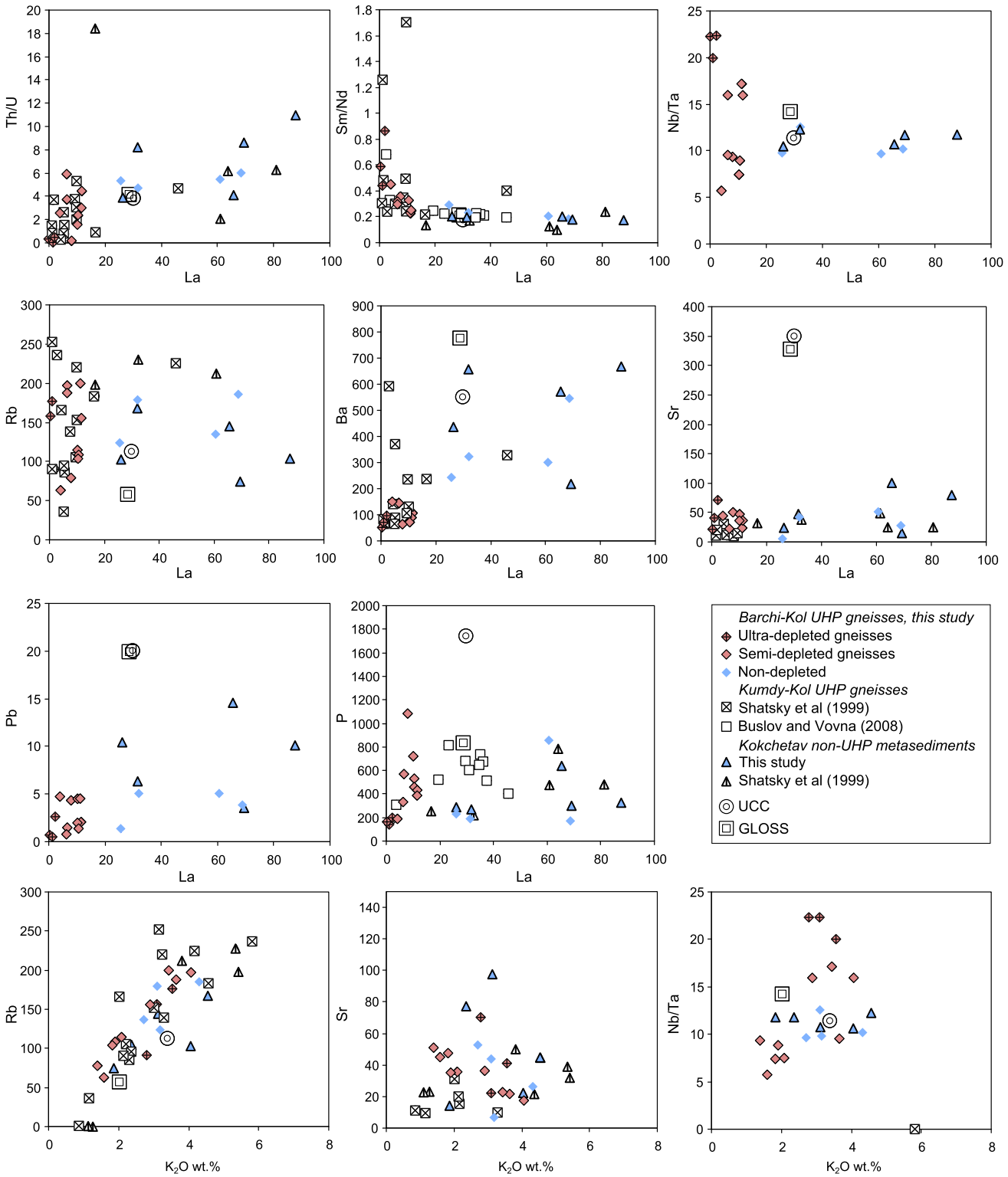

Fig. 7 Concentrations and ratios of selected trace elements in the Kokchetav UHP gneisses compared with non-UHP metasediments, GLOSS (Plank and Langmuir 1998) and UCC (Taylor and McLennan 1985)

Holloway 1988; Vielzeuf and Montel 1994; Schmidt et al. 2004b; Hermann and Spandler 2008). The main constituents of these melts are the felsic components SiO_2–Al_2O_3–Na_2O–K_2O, whereas the mafic components FeO, MgO, CaO are low. An important compositional feature of LREE-depleted rocks from UHP terrains of the Kokchetav

complex is the negative correlation of K_2O and FeO + MgO (Fig. 4c). This trend can be attributed to the variable degree of extraction of a granitic melt with high potassium and low mafic content (Hermann and Spandler 2008). On the other hand, neither a significant depletion of Na_2O and SiO_2 nor enrichment in Al_2O_3 is observed. With increasing pressure, Na_2O becomes increasingly compatible in clinopyroxene (Hermann and Spandler 2008). Experimental melts buffered by phengite and omphacite (Hermann and Spandler 2008) have Na_2O content (2.3–3.8 wt%) and Al_2O_3 comparable to the UHP gneisses from Barchi-Kol and Kumdy-Kol, and SiO_2 is only slightly lower. Hence, melting and melt extraction would not significantly modify the concentration of these elements. Based on this information, the metasedimentary protolith of the UHP metasediments must have had a relatively low Al and elevated Na and Ca contents and thus can be classified as a metagraywacke. Hence, the lower grade metapelites and orthogneisses are unlikely protolith for the diamond-bearing Kokchetav gneisses.

The majority of gneisses from Barchi-Kol we report and the UHP gneisses from the study of Shatsky et al. (1999) show remarkable depletion in LREE, Th and U relative to non-UHP Kokchetav rocks, GLOSS and average continental crust (Fig. 6). The behaviour of LREE during melting is controlled by either monazite or allanite (Hermann and Rubatto 2009). Thus, the solubility of LREE in melts buffered by monazite or allanite serves as an indicator how much LREE can be removed by partial melting. Stepanov et al. (2012) experimentally determined the LREE solubility as a function of pressure, temperature, monazite and melt composition. Temperature is the dominant factor in the LREE solubility, and thus, depletion of these elements can be used to constrain the temperature of melting and melt extraction. At typical crustal melting conditions of 800 °C and 10 kbar, as experienced by the Kokchetav rocks during exhumation, the Σ_{LREE} in the melt is ~360 ppm. In contrast at 1,000 °C, 50 kbar, conditions similar to the peak metamorphism in the Kokchetav gneisses, Σ_{LREE} is ~1,000 ppm. For a protolith with Σ_{LREE} of ~120–200 ppm, 33–55 % of melt extraction is needed at 800 °C, 10 kbar, whereas only 11–18 % is required at 1,000 °C, 50 kbar to produce complete LREE depletion as observed in the ultra-depleted Kokchetav gneisses. This suggests that partial melting and melt extraction at UHP conditions was likely responsible for the LREE depletion. Indeed, unequivocal evidence of melting at UHP conditions was found as quartz–feldspar–diamond aggregates in some gneisses (Korsakov et al. 2004) and melt/polyphase inclusions in diamonds (Hwang et al. 2006) and UHP minerals (Korsakov and Hermann 2006; Stepanov 2012). Therefore, the rocks with LREE depletion represent restites where the composition has been significantly modified by anatexis and melt extraction.

Several samples from Barchi-Kol from this study (B01-3, B94-256, B94-333, B95-99) and the majority of UHP rocks from study by Buslov and Vovna (2008) have LREE contents similar to non-UHP Kokchetav metasediments. It is possible that some or all of those rocks had a different PT path of metamorphism than the restitic gneisses and did not experience melting. Another explanation would be that these rocks have experienced partial melting but did not lose melt and hence their composition remained unmodified. For samples B01-3, B94-256 and B94-333, our unpublished data demonstrate that these rocks likely avoided UHP partial melting (Stepanov 2012).

Influence of residual minerals on the trace element characteristics of UHP gneisses

Garnet

UHP gneisses retain HREE at a level comparable to the Kokchetav non-UHP rocks as well as GLOSS and UCC (Figs. 5, 6). The compatible behaviour of HREE is related to the presence of garnet, which is a common mineral in metasediments at HP/UHP conditions (Auzanneau et al. 2006; Hermann and Spandler 2008) and has high partition coefficients for HREE (Rubatto and Hermann 2007).

Monazite and allanite

Our examination of accessory phases in the studied rocks shows that monazite was present in the unmelted UHP rock (sample B94-333). On the other hand, pseudomorphs after allanite have been observed in sample B118A50. Therefore, we expect that depending on the composition of the protolith that monazite or allanite was present at the onset of UHP anatexis. Experimental investigations have shown that LREE, Th and U are mainly hosted by monazite/allanite and to some extent by zircon at HP–UHP conditions (Klimm et al. 2008; Hermann and Rubatto 2009; Skora and Blundy 2010). Monazite and allanite have quite similar solubility (Klimm et al. 2008) and partitioning properties (Stepanov et al. 2012) with preference of LREE and Th relative to HREE and U. The experimental partitioning data can be used to determine, whether allanite/monazite was a residual phases during melting. With residual monazite/allanite present, LREE + Th are controlled by monazite/allanite solubility, whereas U is incompatible, leading to melts with low Th/U and restites with high Th/U. On the other hand, if monazite/allanite is completely dissolved in the melt, then the melt acquires a major fraction of LREE, Th and U, and residual minerals

control the abundances of these elements in the residue. The ultra-depleted UHP gneisses have extremely low LREE content and much lower Th/U than those of the postulated protolith (Figs. 6, 7). These rocks can be interpreted as restites after efficient extraction of melt in which all monazite/allanite were dissolved. Residual zircon (see below) imposes low Th/U in the ultra-depleted samples. Significant concentrations of LREE, Th and U in the semi-depleted samples can be explained either by the presence of residual monazite/allanite or by contribution of melt, which was not separated from the residue. The absence of samples with substantially elevated Th/U provides evidence that the gneisses did not partially melt at lower temperature in the presence of residual monazite.

Phengite

Phengite is a common mineral in the Kokchetav gneisses. Matrix phengite has low Si and Ti contents, indicating formation during retrogression (Massonne 2003; Auzanneau et al. 2010). Phengite is also observed as inclusions in garnet and zircon, where it can be intergrown with metamorphic diamonds (Vavilov et al. 1993; Katayama and Maruyama 2009). The mica inclusions have high Si and Ti concentrations (Hermann et al. 2001; Korsakov and Hermann 2006; Katayama and Maruyama 2009) indicating a HT and UHP origin (Hermann and Spandler 2008; Auzanneau et al. 2010). K minerals are consumed at the onset of HP melting in mafic rock compositions (Rapp et al. 1991; Kiseeva et al. 2012). However, in metasediments, white mica is stable at HP with melt over a wide range of temperatures (Auzanneau et al. 2006; Hermann and Spandler 2008). Therefore, phengite was present at peak conditions in at least some of the Kokchetav rocks. Phengite is the major host for LILE (K, Rb, Ba) in metasedimentary rocks (Bebout et al. 1993; Hermann 2002; Hermann and Rubatto 2009). The ultra-depleted samples from this study have still significant K_2O contents (2.8–3.5 wt%) and considering that melt was efficiently extracted from these rocks (see above), we conclude that they contained some residual phengite. High-pressure experiments in pelitic rocks have shown that Rb is compatible in phengite ($D = 1.5$) at 4.5 GPa, 900–1,000 °C, whereas Ba ($D = 0.5$) and Cs ($D = 0.15$) are incompatible (Hermann, unpublished data). This can partly explain the observed correlation of Rb and K_2O in LREE-depleted gneisses and the decoupling of Rb from Ba. Phengite can be a significant host for Nb and Ta and it prefers Nb over Ta (Stepanov and Hermann 2013). Therefore, the elevated Nb/Ta of the ultra-depleted samples provides further evidence for residual phengite in our samples.

A number of samples in the study of Shatsky et al. (1999) have $K_2O < 1.2$ % coupled with low Rb, Cs and Sr concentrations. These samples clearly were depleted in K, other LILE as well as in LREE and Th. In those samples, phengite completely melted out and melt was efficiently extracted. This resulted in anhydrous restite composed of garnet, coesite ± pyroxene. None of our samples have a composition similar to the LILE-depleted samples from Shatsky et al. (1999). Therefore, the absence of large depletion of Sr and Cs in LREE-depleted gneisses could be attributed to a relatively high fraction of residual melts with high Sr and Cs contents in the majority of our samples.

Rutile

Nb and Ta are geochemically similar elements and are commonly concentrated in Ti-bearing minerals such as rutile, titanite and ilmenite. These minerals preferentially incorporate Ta over Nb (Schmidt et al. 2004a; Xiong et al. 2011). Rutile is a common accessory phase in the studied UHP rocks (Table 1) where it might have formed either as peak metamorphic mineral or during exhumation by release of titanium from mica and garnet. In eclogites with high Ti and low K contents, rutile is the main host for Nb and Ta (Hermann 2002). However, in UHP metasediments with much higher K_2O contents of up to 4 wt% and lower TiO_2 contents of 0.45–0.65 wt% (BA118 series, B01-3; Table 2), 25–40 % of modal phengite containing 2–2.5 wt% TiO_2 can be the major Ti-bearing phase. Recently, phengite and biotite were recognized as significant hosts for Nb and Ta (Stepanov and Hermann 2013) and UHP phengite found as inclusions in Kokchetav zircons contains 2–3 wt% of TiO_2 (Hermann et al. 2001). Because Ta is favoured by rutile and Nb by phengite, the Nb/Ta can provide additional information on which of these two minerals was the dominant Ti phase in the restite. Kokchetav non-UHP rocks and Barchi-Kol samples without LREE depletion demonstrate consistent Nb/Ta of 9.6–12, which are close to Nb/Ta of 12–13 in UCC (Barth et al. 2000). However, about half of the LREE-depleted samples display much higher Nb/Ta up to 24, providing evidence for phengite in the restite. The other half of the samples has a lower Nb/Ta, and we suggest that in these rocks residual rutile was the dominant host for Nb and Ta. All ultra-depleted samples have high Nb/Ta, suggesting the presence of residual phengite. Therefore, the increasing variability of Nb/Ta with decreasing La (Fig. 7) is interpreted as a result of the different proportions of residual phengite and rutile during partial melting.

Zircon

Zircon is a common mineral in the Kokchetav gneisses, and it hosts inclusions of UHP minerals such as garnet,

phengite and diamond (Sobolev et al. 1991; Vavilov et al. 1993; Hermann et al. 2001; Katayama et al. 2001) indicating that it was a residual phase at UHP conditions. Zircon is the main host of Zr in felsic UHP rocks, and the solubility of Zr in the melt will govern Zr enrichment or depletion during partial melting (Hermann and Rubatto 2009). Zr concentrations are similar in most of the UHP gneisses and in the non-UHP metasediments from the Kokchetav complex (Table 2), with the exception of sample B94-355, which has a particularly low Zr content of 77 ppm. Zr/Hf is also similar in UHP gneisses, the Kokchetav non-UHP metasediments and the average continental crust (Taylor and McLennan 1985). Therefore, Zr and Hf were neither depleted nor fractionated or increased during UHP melting (because there is no correlation between Zr and Fe + Mg). This zero effect of melt extraction can be explained by similar concentrations of Zr in the melt and in the bulk rock. The solubility of zircon in a melt is strongly temperature dependent (Watson and Harrison 1983) and is not affected by pressure (Boehnke et al. 2013). The Zr + Hf content in melts produced from metapelites and buffered by zircon at 1,000 °C and 45 kbar is 260 ppm (Hermann and Rubatto 2009), similar to the Zr concentrations in the non-UHP samples and the UHP gneisses. Extraction of melts with 200–300 ppm Zr would neither decrease nor increase the Zr content in the residue but if the temperature was significantly higher than 1,000 °C, then zircon solubility would be higher and Zr would behave as an incompatible element. Therefore, the Zr behaviour provides additional constraints that, when melt extraction occurred, temperatures did not significantly exceed 950–1,000 °C. Zircon in equilibrium with melt has a strong preference for U and HREE relative to Th and LREE (Rubatto and Hermann 2007). As residual metamorphic zircon is the main host for Th and U in the restites, this can explain the low Th/U of the ultra-depleted samples.

Apatite

Both the non-UHP samples and the UHP gneisses show low and overlapping phosphorous contents. LREE and phosphorous in UHP gneisses with low LREE content (<35 ppm, Fig. 7) show a positive correlation, and in the ultra-depleted samples, the phosphorous content is as low as 130–170 ppm. Samples with higher LREE content show a large variation in phosphorous content, and samples with the highest phosphorous content contain apatite (B94-57). This variation in phosphorous can be explained by the incompatible behaviour of phosphorous during melting and complete dissolution of apatite in the melt. Indeed, phosphorous contents in melts saturated in apatite at 1,000 °C and 45 kbar are 1,350 ppm (Hermann and Spandler 2008). In more mafic compositions, as those investigated in experiments by Green and Adam (2002), phosphorous in melts buffered by apatite is as high as ≈1 wt%. Therefore, 20 % melting would be sufficient to dissolve all apatite in rocks with 270 ppm P. The ultra-depleted samples still contain ≈150 ppm of phosphorous. This minor amount can be explained by the high solubility of phosphorous in garnet at such conditions (up to 3,000 ppm; Hermann and Spandler 2008). Hence, even efficient melt extraction results in incomplete depletion in phosphorous and can result in a decoupling of this element from LREE.

Sulphides

The sulphur content measured by XRF was above detection limit only in four samples with a maximum SO_3 of 0.9 wt% in sample B94-57 (Table 2). These small number of samples display a positive correlation between S and Sb, As and Zn concentrations. Hermann et al. (2006) proposed that sulphide melt immiscibility with silicate and carbonatitic melt existed at UHP conditions in some of the Kokchetav rocks. This melt is expected to have a high density and therefore might sink through the host rock and could scavenge chalcophile elements. Such a process could explain the positive correlation of S with chalcophile elements.

Possibility of other restitic phases

The proposed set of restitic minerals and different efficiency of melt extraction provide an explanation for the behaviour of the majority of trace elements; however, a number of questions remains particularly regarding mobile elements such as Sr, Cs and Pb. Experimental studies reported Sr as one of the most incompatible elements during high pressure melting of metasediments (Hermann and Rubatto 2009; Martindale et al. 2013). The Kokchetav restitic rocks are not depleted in Sr with respect to the protolith. However, it is worth noting that the overall Sr content of all Kokchetav gneisses is an order of magnitude lower than in average crustal rocks (Fig. 6). Omphacite has been found as inclusion in UHP domains of zircon from gneisses (Hermann et al. 2001) indicating that it was a residual phase. Thus, omphacite is a potential host for Sr in the gneisses. Carbonates are important minerals in several types of the Kokchetav rocks. Aragonite is stable at UHP conditions in carbonate-bearing metasediments (Korsakov et al. 2009, 2011) and is potentially an important host for Sr. Cs is less compatible in muscovite than Rb (Icenhower and London 1995); however, the ultra-depleted gneisses do not show a large Rb-Cs fractionation hence rising questions regarding LILE partitioning between phengite and melt at UHP conditions. Pb is less depleted than LREE in many

UHP rocks resulting in a positive Pb-anomaly (Fig. 6). Lead could be hosted by a number of phases such as phengite or sulphides.

Comparison of Kokchetav UHP gneisses with other crustal restites

The restitic UHP gneisses of the Kokchetav complex were formed from a metasedimentary protolith by extraction of partial melts. Other lithologies in the Kokchetav complex also show evidence of partial melting; for instance, marbles and garnet-pyroxene rocks contain inclusions of carbonatitic and silicate melts (Korsakov and Hermann 2006). Shatsky et al. (1999) reported a trondhjemite vein possibly formed by melting of eclogite. Therefore, different lithologies at the Barchi-Kol and Kumdy-Kol UHP terrains experienced melting and the terrains can be classified as neosome migmatites (Sawyer 2008).

The geochemical features of the Kokchetav UHP gneisses are distinct from typical crustal migmatites. In the Kokchetav UHP gneisses, LREE, Th and U are strongly depleted and the effect of UHP melting on HFSE and LILE concentrations is less significant. In contrast, crustal restites, which experienced partial melting at granulite facies conditions, commonly show depletion in Rb and U (Rollinson and Windley 1980; Nozhkin and Turkina 1993), whereas REE and Th concentrations are not affected (Rollinson and Windley 1980; Guernina and Sawyer 2003). The lower crustal migmatites of the Ivrea-Verbano zone show significant depletion in Rb, Cs, Bi, Tl, Li and U and moderate depletion in P, Pb, K and Na but no depletion in LREE and Th (Schnetger 1994; Bea and Montero 1999). The depletion of U relative to Th in crustal migmatites is due to extraction of melts in the presence of residual monazite (Stepanov et al. 2012). In the Kokchetav complex, monazite was completely dissolved in the melt and this resulted in simultaneous extraction of LREE, Th and U.

The composition of the Kokchetav UHP gneisses is different from typical crustal migmatites due to melting of crustal rocks at ultra-high temperatures (UHT; $T \geq 950$ °C) when the host phase for LREE, Th and U (monazite/allanite) was completely dissolved in the melt that is efficiently extracted. This type of melting has important geochemical implications: it produces large fractionation of LREE, Th and U from other incompatible trace elements, and melting results in the redistribution of heat producing elements (Th, U and partially K), which does not occur in typical anatexis of continental crust at 800 °C. Ewing et al. (2014) described UHT pelitic enclaves (septa) in gabbros from the Ivrea-Verbano zone that were heated to 1,000–1,050 °C and experienced significant melt extraction. Some septa display depletion in LREE, Th and U comparable to the Kokchetav gneisses that is accompanied by a strong depletion in LILE. On the other hand, UHT rocks from Antarctica commonly do not show depletion in LREE (Grew et al. 2006). The absence of LREE depletion in some UHT rocks might be related to dehydration and melt extraction during previous granulite metamorphism, which might limit melting at UHT conditions (Vielzeuf et al. 1990).

The rocks from the Saxonian Erzgebirge, Germany, are regarded as another example of melting of metasediments at UHP/UHT conditions (Massonne 2003; Behn et al. 2011). Bulk rock compositions from these rocks reported by Behn et al. (2011) show highly variable LREE concentrations: in some samples, La is clearly depleted, whereas others show no LREE depletion. Th/U varies widely (from 0.35 to 36), and the scatter of Nb/Ta is also significant (from 4.5 to 25). These features suggest that the Erzgebirge rocks might also represent restites in which dissolution or preservation of monazite, zircon, rutile and phengite controlled their trace element compositions similarly to the Kokchetav rocks.

Restites with chemical characteristics similar to the ultra-depleted Kokchetav gneisses are occasionally found as xenolithes in alkaline volcanoes. Mazzone and Haggerty (1989) proposed that specific xenoliths in kimberlites such as alkremite (garnet + spinel), corganite (corundum + garnet) and corgaspinite (corundum + garnet + spinel) were formed after melting and melt extraction of metasediments. These rocks are extremely enriched in Al_2O_3 and depleted in SiO_2 and alkalies. Ultrapotassic igneous rocks in the southern Pamir (Tajikistan) contain xenoliths of granulites and eclogites (Hacker et al. 2005). These rocks originate from the slab subducted beneath the Asian plate during the collision of India and Asia (Ducea et al. 2003; Hacker et al. 2005) and experienced metamorphic conditions in the range of 875–1,100 °C and 20–29 kbar (Hacker et al. 2005). The Pamir metasedimentary xenoliths with the highest peak conditions experienced melting as evident from melt inclusions in various minerals (Chupin et al. 2006; Madyukov et al. 2011). Samples metamorphosed at temperature in excess of 900 °C show evidence for depletion in La, Th and Ba (Gordon et al. 2011) and thus may record melting at extreme conditions similar to the Kokchetav rocks.

Implications

Fate of the melts derived from the UHP gneisses

Rocks of igneous origin in the Kokchetav metamorphic belt are dominated by granites and granitic orthogneisses, though some minor intrusions of gabbros, pyroxenites and

carbonatites are present. Orthogneisses are abundant in the Kokchetav complex, and they are considered to represent the basement of the Kokchetav continent (Dobretsov et al. 2006; Turkina et al. 2011). Notable localities include outcrops near the Kulet lake (Kushev and Vinogradov 1978), Chaglinskoe water reservoir (Turkina et al. 2011) and Kumdy-Kol lake (Kushev and Vinogradov 1978). U–Pb dating of zircons from these magmatic rocks yielded ages of 1,128–1,169 Ma (Letnikov et al. 2007; Turkina et al. 2011; Tretyakov et al. 2011). The Zerenda batholith at the southern boundary of the Kokchetav complex formed at 460–440 Ma (Shatagin et al. 1999, 2001). Therefore, major intrusions of the Kokchetav belt predate and postdate UHP metamorphism and cannot be related to this event and, thus, do not represent partial melts derived from melting of the Kokchetav UHP gneisses.

Trondhjemite veins in eclogites reported in the Kumdy-Kol terrain by Shatsky et al. (1999) are the only magmatic rocks of the same age as UHP metamorphism. The trondhjemites are rich in Na_2O and have a low LREE content (La 10 ppm) and thus cannot represent UHP melts extracted from metasediments. Therefore, rocks equivalent to the partial melts derived from the UHP gneisses are unknown at the present level of exposure.

Geochemical signature of melts derived from subducted crustal rocks

Depletion in trace elements of the UHP gneisses during partial melting coincides with complementary enrichment of extracted melts. Based on the geochemical characteristics of the studied restites, we are able to constrain some main features of the extracted melts: (1) the major element composition of the melts resembles potassium rich peraluminous granites. (2) The melts have high LREE contents and strongly fractionated REE patterns. (3) Th/U and Th/La are similar to those of their protolith and UCC, because monazite/allanite was completely dissolved in the melts (Skora and Blundy 2010; Stepanov et al. 2012). (4) Such melts have moderate enrichment in LILE and HFSE, despite phengite and rutile being stable in the restite, because the crustal source sediments has high LILE and HFSE. (5) Low Nb/Th and Nb/U and high Ba/Nb are characteristic because Nb is moderately compatible in the residue, whereas Ba, LREE, Th and U are highly enriched in the melt. (6) The Ba/La remains close to those of the protolith sediments. All these features render UHP partial melts significantly different form crustal granites formed at low pressures (Condie 1993).

The Kokchetav massif is one of a few places worldwide where partial melting of deeply subducted sediments can be studied directly. The pressure of partial melting in the Kokchetav massif is comparable to where sediment melting is expected at sub-arc depth in subduction zones (Hermann and Spandler 2008), although the melting temperature in the Kokchetav rocks was considerably higher than what was commonly predicted for subduction systems. Nevertheless, the chemical signature of Kokchetav restites has been used to explain the trace element composition of arc lavas and to infer the mechanism of transport from the slab to the arc (Behn et al. 2011; Hacker et al. 2011). Behn et al. (2011) proposed that 100 % of Th in subducted sediments is recycled back to the continental crust by arc magmatism and proposed that the sedimentary component is transferred to the mantle by diapirs, which experienced high degrees of melting. This model was illustrated by the intensive Th depletion in the Kokchetav gneisses, and Behn et al. (2011) proposed that the majority of subducted sediments undergo melting in conditions similar to that of the Kokchetav rocks. However, our study shows that melting in the Kokchetav rocks produces quite distinct chemical characteristics that are different from the subduction component of arc lavas.

Island arcs basalts have a number of characteristics, which are considered as contributions from subducted sediments: (1) high LILE contents with moderate LREE concentrations (Hermann and Green 2001), (2) low Th/U and Th/La similar to those of subducted sediments (Taylor and McLennan 1985; Plank and Langmuir 1998; Plank 2005), (3) low Nb/Th and Nb/U (Ryerson and Watson 1987), (4) low Ce/Pb (Taylor and McLennan 1985). These features are consistent with water assisted melting, with monazite/allanite as residual mineral and occurring at significantly lower temperatures than melting in the Kokchetav complex (Spandler and Pirard 2013). UHP melts produced from melting of the Kokchetav gneisses differ from arc magmas by high contents of LREE, modest contents of LILE and high Th/U. In the Kokchetav rocks, Pb was less depleted than LREE and melts had high Ce/Pb. Therefore, it is unlikely that Kokchetav-type melts are the direct source of the crustal signature in arc magmas.

The magmas related to the Kokchetav-type melting might be represented by some high-K magmas (shoshonites) observed in orogenic belts (Turner et al. 1996). For example, shoshonites in Eastern Tibet display high K_2O concentrations, high K_2O/Na_2O ratios and very high LREE concentrations (La 300–500 ppm; Campbell et al. 2014). These authors suggested that the primary melts for shoshonites were formed by high degree melting (20–40 %) of crustal rocks. Melting at high temperature, high-pressure conditions resulted in the complete dissolution of monazite, phengite and probably zircon in the melt. The interaction of such felsic melts with peridotites of the mantle then produced a suite of K-rich rocks ranging from mafic and ultramafic to felsic members. The whole rock suite displays

a similar trace element signature that is consistent with geochemical features of the melts produced by UHP anatexis of the Kokchetav gneisses.

Implications for the isotopic signature of enriched mantle reservoirs

It is widely accepted that Earth can be subdivided into reservoirs with distinct isotopic compositions such as the depleted mantle, continental crust, HIMU mantle (with high $^{238}U/^{204}Pb$, μ) and others (Zindler and Hart 1986). Usually, these reservoirs are linked to subducted crustal material (Zindler and Hart 1986; Chauvel et al. 2008) though explanations based on mantle convection are also proposed (Kostitsyn 2007). The continental crust is characterized by low $^{143}Nd/^{144}Nd$ and $^{176}Hf/^{177}Hf$, and high $^{86}Sr/^{87}Sr$. It has been proposed that basalts with such isotopic signature might derive from a mantle reservoirs contaminated by subducted crustal material. In order to calculate the proportion of crustal contamination into mantle-derived melts, it is assumed that the crustal material does not significantly change its isotopic ratio during subduction (Chauvel et al. 2008). However, our study on the Kokchetav UHP gneisses demonstrates that subduction melting can induce dramatic changes in the composition of crustal rocks, which affects principal element ratios pertinent to their isotopic evolution.

The Kokchetav restites are rich in garnet, and thus, they might reach a density greater than the surrounding mantle. UHP anatexis and melt extraction from a metagraywacke results in restite with high MgO + FeO + CaO of 12.4–19 wt%. Garnet is the main host of these elements in the restite. Using the garnet composition included in UHP zircon from Barchi-Kol given by Hermann et al. (2001) (MgO + FeO + CaO 35–38.5 wt%), this results in high modal garnet of 30–50 %. Considering the high density of such garnets of 4.1 g/cm^3 and a minimum density of 3.0 g/cm^3 for other rock forming minerals (phengite, coesite, rutile, omphacite), the resulting bulk density of such restites is between 3.3 and 3.5 g/cm^3. This is close to the bulk density of the mantle (3.2–3.4 g/cm^3). Thus, UHP rocks that underwent significant extraction of buoyant melt and that are not coupled with less dense rock types (e.g. gneisses) may be able to sink into the deeper mantle and might contribute to its isotopic heterogeneity (Hacker et al. 2011). In the following, we speculate on the type of isotopic signatures that would develop if the Kokchetav UHP restites would remain in the mantle for an extensive period of time.

The UHP melting of Kokchetav metasediments caused a strong decoupling of LREE from HREE and, in particular, fractionated Sm from Nd (Fig. 7). While Nd partitioned into the melt, Sm remained in garnet, causing >50 % increase in the Sm/Nd ratio in the semi-depleted samples and up to 400 % increase in the ultra-depleted samples. Therefore, the decay of the ^{147}Sm remaining in the UHP restites is expected to produce high $^{143}Nd/^{144}Nd$ ratios over time. In contrast to the Sm–Nd system, the Lu–Hf system appears to be relatively unaffected by UHP melting leading to a decoupling of Lu–Hf and Sm–Nd systems. The effect of UHP melting on the Rb–Sr system is somewhat unclear. In our samples, evidence for systematic Rb–Sr depletion and/or fractionation are not apparent. However, Shatsky et al. (1999) proposed that the amount of radiogenic Sr is not supported by the Rb concentrations.

The Kokchetav UHP restites have high concentrations of incompatible elements in comparison with the mantle. If the Kokchetav restites were to be mixed into the mantle, they would produce reservoirs with high incompatible element content, particularly the LILE and HFSE. Such a reservoir would have crust-like Sr and Hf isotopic composition but its Nd isotopic composition will be different. With time, the restite after UHP melting would move away from the main terrestrial evolution line in the $^{143}Nd/^{144}Nd$—$^{176}Hf/^{177}Hf$ space to highly radiogenic $^{143}Nd/^{144}Nd$ values (Fig. 8). Particularly important is that the Nd isotopic composition could evolve to high values, which could resemble depleted mantle-like values. Therefore, the storage of Kokchetav-like restites in the mantle could produce a source with quite specific isotopic characteristics.

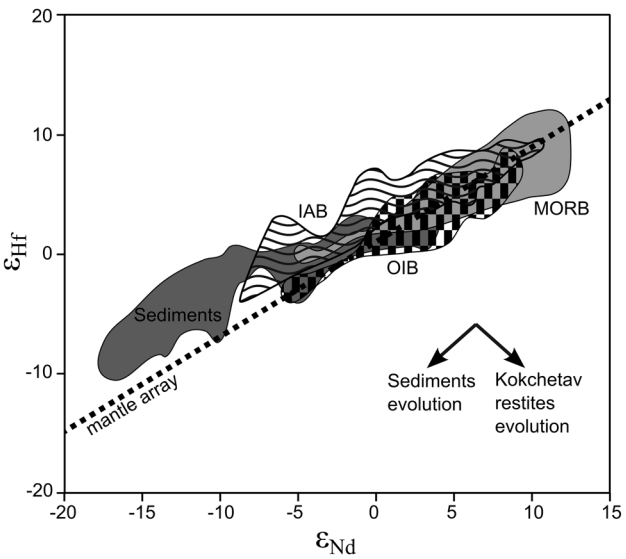

Fig. 8 Sm–Nd and Lu–Hf systematics of subducted sediments, MORB, arc magmas and oceanic island basalts (OIB) according to Chauvel et al. (2008). Restites after Kokchetav-type melting evolve to higher ε_{Nd} and closer to the mantle array because of fractionation of Sm and Nd. See text for discussion

MORB and OIB generally show a good correlation between $^{143}Nd/^{144}Nd$ and $^{176}Hf/^{177}Hf$ or ε_{Nd} and ε_{Hf} (Zindler and Hart 1986; Chauvel et al. 2008). Oceanic sediments generally have lower ε_{Nd} and ε_{Hf} and plot above the mantle array (Fig. 8). Chauvel et al. (2008) proposed that Lu–Hf and Sm–Nd systems of subducted sediments and oceanic crust are not affected by subduction and calculated that OIB might contain 0–6 % and MORB 0–2.2 % of a recycled sediment component. However, the decoupling of these systems during UHP melting, as shown in this study, implies that with time the restite, after melting of metasediment, will evolve to high ε_{Nd} values at relatively constant or decreasing ε_{Hf}. This will bring the restites closer to the terrestrial evolution line, and thus, the contribution of restites after melting of metasediments could be higher than estimated by Chauvel et al. (2008).

Conclusion

The study of bulk rock geochemistry of the Kokchetav gneisses provides insights into melting at UHP conditions:

- The UHP gneisses of the Kokchetav complex derive from metagraywacke protoliths that experienced melting and melt extraction at UHP conditions, which significantly affected their major and trace element compositions.
- During UHP melting of the Kokchetav metasediments, LREE, Th and U were strongly incompatible, whereas LILE, Nb, Ta and P were moderately incompatible elements. Zr and Hf contents remained unchanged. The depletion of LREE was caused by complete dissolution of monazite/allanite in melts and the loss of granitic melts with high LREE content, whereas some of the LILE were retained in residual phengite. There was no fractionation of Th from U and LREE from Th during melt extraction because all monazite/allanite was dissolved in the melt. The LREE and Zr contents of the restite constrain the temperature of melting to $\sim$1,000 °C.
- LREE, Th and U in moderately depleted UHP gneisses derive from melt that was not efficiently extracted. Residual zircon in samples that experienced efficient melt extraction resulted in restites with U > Th.
- Anatexis generated granitic melts with high LREE, Th and U contents and moderate LILE and HFSE abundances. These features are different from trace element signatures of arc lavas, and thus, Kokchetav-type melting is unlikely to be a main source of crustal components in arc basalts. The role of such melts in mantle wedge metasomatism requires further evaluation.
- Melting of metasediments at UHP conditions results in a large fractionation of key parent/daughter trace element ratios. The observed increase in Sm/Nd and constant value of Lu/Hf in restites with respect to the protolith results in decoupling of the Sm–Nd from the Lu–Hf isotope systems. Over time the restites will develop isotopic compositions significantly different from modern continental crust, which has implications for the evolution of mantle isotopic reservoirs.

Acknowledgments We thank Ulrike Troitzsch and Esme Spicer for analytical assistance and Carl Spandler for valuable suggestions, comments and corrections. Jesse Jones, Seann McKibbin, Paolo Sossi, Paul Millsteed, Jason Doull and Kate Boston are thanked for correction of the manuscript at various stages. The constructive reviews by H.P. Schertl, Y. Xiao and an anonymous reviewer helped to improve the paper. We would like to thank J. Hoefs for the efficient handling of our manuscript. The study was supported by ARC grant DP0556700, RFBR grant 13-05-00367 and Grant of the President of Russia MD-1260.2013.5 and Grant of Ministry of Education of Russia.

References

Auzanneau E, Vielzeuf D, Schmidt MW (2006) Experimental evidence of decompression melting during exhumation of subducted continental crust. Contrib Mineral Petrol 152:125–148. doi:10.1007/s00410-006-0104-5

Auzanneau E, Schmidt MW, Vielzeuf D, Connolly JAD (2010) Titanium in phengite: a geobarometer for high temperature eclogites. Contrib Mineral Petrol 159:1–24. doi:10.1007/s00410-009-0412-7

Barth MG, McDonough WF, Rudnick RL (2000) Tracking the budget of Nb and Ta in the continental crust. Chem Geol 165:197–213

Bea F (1996) Residence of REE, Y, Th and U in granites and crustal protoliths; implications for the chemistry of crustal melts. J Pet 37:521–552

Bea F, Montero P (1999) Behavior of accessory phases and redistribution of Zr, REE, Y, Th, and U during metamorphism and partial melting of metapelites in the lower crust: an example from the Kinzigite Formation of Ivrea-Verbano, NW Italy. Geochim Cosmochim Acta 63:1133–1153

Bebout GE, Ryan J, Leeman W (1993) B-Be systematics in subduction-related metamorphic rocks—characterization of the subducted component. Geochim Cosmochim Acta 57:2227–2237

Bebout GE, Ryan J, Leeman W, Bebout A (1999) Fractionation of trace elements by subduction-zone metamorphism—effect of convergent-margin thermal evolution. Earth Planet Sci Lett 171:63–81

Bebout GE, Bebout AE, Graham CM (2007) Cycling of B, Li, and LILE (K, Cs, Rb, Ba, Sr) into subduction zones: SIMS evidence from micas in high-P/T metasedimentary rocks. Chem Geol 239:284–304. doi:10.1016/j.chemgeo.2006.10.016

Behn MD, Kelemen PB, Hirth G, Hacker BR, Massonne H-J (2011) Diapirs as the source of the sediment signature in arc lavas. Nat Geosci 4:641–646. doi:10.1038/ngeo1214

Boehnke P, Watson EB, Trail D, Harrison TM, Schmitt AK (2013) Zircon saturation re-revisited. Chem Geol 351:324–334. doi:10.1016/j.chemgeo.2013.05.028

Buslov MM, Vovna GM (2008) Composition and geodynamic nature of the protoliths of diamondiferous rocks from the Kumdy-Kol deposit of the Kokchetav metamorphic belt, northern Kazakhstan. Geochem Int 46:887–896. doi:10.1134/S0016702908090036

Buslov MM, Zhimulev FI, Travin AV (2010) New data on the structural setting and Ar-40/Ar-39 age of the MP-LP metamorphism of the Daulet formation, Kokchetav metamorphic belt, Northern Kazakhstan, and their tectonic interpretation. Dokl Earth Sci 434:1147–1151. doi:10.1134/S1028334X10090023

Campbell IH, Stepanov AS, Liang H-Y, Allen CM, Norman MD, Zhang Y-Q, Xie Y-W (2014) The origin of shoshonites: new insights from the Tertiary high-potassium intrusions of eastern Tibet. Contrib Mineral Petrol 167:1–22

Chauvel C, Lewin E, Carpentier M, Arndt NT, Marini J-C (2008) Role of recycled oceanic basalt and sediment in generating the Hf-Nd mantle array. Nat Geosci 1:64–67

Chopin C, Brunet F, Gebert W, Medenbach O, Tillmanns E (1993) Bearthite, Ca2Al[PO4]2(OH), a new mineral from high-pressure terranes of the Western Alps. Schweiz Miner Petrogr Mitt 73:1–9

Chupin VP, Kuz'min DV, Madyukov IA (2006) Melt inclusions in minerals of scapolite-bearing granulite (lower crustal xenoliths from diatremes of the Pamirs). Dokl Earth Sci 407:507–511

Claoue-Long J, Sobolev N, Shatsky V, Sobolev A (1991) Zircon response to diamond-pressure metamorphism in the Kokchetav massif, USSR. Geology 19:710–713

Condie K (1993) Chemical-composition and evolution of the upper continental-crust—contrasting results from surface samples and shales. Chem Geol 104:1–37

Dobretsov NL, Sobolev NV, Shatsky VS, Coleman RG, Ernst WG (1995) Geotectonic evolution of diamondiferous paragneisses of the Kokchetav Complex, Northern Kazakhstan—the geologic enigma of ultrahigh-pressure crustal rocks within Phanerozoic foldbelt. Isl Arc 4:267–279

Dobretsov NL, Buslov MM, Zhimulev FI, Travin A, Zayachkovsky A (2006) Vendian-early Ordovician geodynamic evolution and model for exhumation of ultrahighand high-pressure rocks from the Kokchetav subduction-collision zone (northern Kazakhstan). Russ Geol Geophys 47:424–440

Ducea M, Lutkov V, Minaev V, Hacker B, Ratschbacher L, Luffi P, Schwab M, Gehrels G, McWilliams M, Vervoort J, Metcalf J (2003) Building the pamirs: the view from the underside. Geology 31:849–852

Eggins SM, Rudnick RL, McDonough WF (1998) The composition of peridotites and their minerals: a laser-ablation ICP-MS study. Earth Planet Sci Lett 154:53–71. doi:10.1016/S0012-821X(97)00195-7

Ewing TA, Rubatto D, Hermann J (2014) Hafnium isotopes and Zr/Hf of rutile and zircon from lower crustal metapelites (Ivrea–Verbano Zone, Italy): implications for chemical differentiation of the crust. Earth Planet Sci Lett 389:106–118. doi:10.1016/j.epsl.2013.12.029

Gilbert AE, Kozmenko OA, Shatskiy VS (1990) Rare and rare-earth elements in Kokchetau Massif eclogites. Geochem Int 27:133–137

Glorie S, Zhimulev FI, Buslov MM, Andersen T, Plavsa D, Izmer A, Vanhaecke F, De Grave J (2013) Formation of the Kokchetav subduction–collision zone (northern Kazakhstan): Insights from zircon U-Pb and Lu–Hf isotope systematics. Gondwana Res. doi:10.1016/j.gr.2013.10.012

Gordon S, Kelemen P, Hacker B, Luffi P, Ratschbacher L (2011) Partial melting and its role in elemental recycling: insight from pamir metasedimentary xenoliths. Goldschmidt Conf. 2011 Abstr. p 937

Green T, Adam J (2002) Pressure effect on Ti- or P-rich accessory mineral saturation in evolved granitic melts with differing K_2O/Na_2O ratios. Lithos 61:271–282

Guernina S, Sawyer EW (2003) Large-scale melt-depletion in granulite terranes: an example from the Archean Ashuanipi subprovince of Quebec. J Metamorph Geol 21:181–201. doi:10.1046/j.1525-1314.2003.00436.x

Hacker B, Calvert A, Zhang R, Ernst W, Liou J (2003) Ultrarapid exhumation of ultrahigh-pressure diamond-bearing metasedimentary rocks of the Kokchetav Massif, Kazakhstan? Lithos 70:61–75. doi:10.1016/S0024-4937(03)00092-6

Hacker B, Luffi P, Lutkov V, Minaev V, Ratschbacher L, Plank T, Ducea M, Patino-Douce A, McWilliams M, Metcalf J (2005) Near-ultrahigh pressure processing of continental crust: miocene crustal xenoliths from the Pamir. J Pet 46:1661–1687

Hacker BR, Kelemen PB, Behn MD (2011) Differentiation of the continental crust by relamination. Earth Planet Sci Lett 307:501–516. doi:10.1016/j.epsl.2011.05.024

Hermann J (2002) Allanite: thorium and light rare earth element carrier in subducted crust. Chem Geol 192:289–306

Hermann J, Green DH (2001) Experimental constraints on high pressure melting in subducted crust. Earth Planet Sci Lett 188:149–168

Hermann J, Rubatto D (2009) Accessory phase control on the trace element signature of sediment melts in subduction zones. Chem Geol 265:512–526

Hermann J, Rubatto D (2014) 4.9—subduction of continental crust to mantle depth: geochemistry of ultrahigh-pressure rocks. In: Holland HD, Turekian KK (eds) Treatise on geochemistry, 2nd edn. Elsevier, Oxford, pp 309–340

Hermann J, Spandler CJ (2008) Sediment melts at sub-arc depths: an experimental study. J Pet 49:717–740

Hermann J, Spandler C, Hack A, Korsakov AV (2006) Aqueous fluids and hydrous melts in high-pressure and ultra-high pressure rocks: Implications for element transfer in subduction zones. Lithos 92:399–417

Hermann J, Rubatto D, Korsakov A, Shatsky VS (2001) Multiple zircon growth during fast exhumation of diamondiferous, deeply subducted continental crust (Kokchetav Massif, Kazakhstan). Contrib Mineral Petrol 141:66–82

Hwang S-L, Chu H-T, Yui T-F, Shen P, Schertl H-P, Liou JG, Sobolev NV (2006) Nanometer-size P/K-rich silica glass (former melt) inclusions in microdiamond from the gneisses of Kokchetav and Erzgebirge massifs: diversified characteristics of the formation media of metamorphic microdiamond in UHP rocks due to host-rock buffering. Earth Planet Sci Lett 243:94–106. doi:10.1016/j.epsl.2005.12.015

Icenhower J, London D (1995) An experimental study of element partitioning among biotite, muscovite, and coexisting peraluminous silicic melt at 200 MPa (H_2O). Am Miner 80:1229–1251

Jochum KP (2011) Determination of reference values for nist srm 610-617 glasses following iso guidelines. Geostand Geoanal Res 35:397–429

John T, Scherer EE, Haase K, Schenk V (2004) Trace element fractionation during fluid-induced eclogitization in a subducting slab: trace element and Lu–Hf–Sm–Nd isotope systematics. Earth Planet Sci Lett 227:441–456

Kaneko Y, Maruyama S, Terabayashi M, Yamamoto H, Ishikawa M, Anma R, Parkinson CD, Ota T, Nakajima Y, Katayama I, Yamamoto J, Yamauchi K (2000) Geology of the Kokchetav UHP–HP metamorphic belt, Northern Kazakhstan. Isl Arc 9:264–283

Katayama I, Maruyama S (2009) Inclusion study in zircon from ultrahigh-pressure metamorphic rocks in the Kokchetav massif: an excellent tracer of metamorphic history. J Geol Soc 166:783–796. doi:10.1144/0016-76492008-019

Katayama I, Maruyama S, Parkinson C, Terada K, Sano Y (2001) Ion micro-probe U-Pb zircon geochronology of peak and retrograde stages of ultrahigh-pressure metamorphic rocks from the

Kokchetav massif, northern Kazakhstan. Earth Planet Sci Lett 188:185–198

Kiseeva ES, Yaxley GM, Hermann J et al (2012) An experimental study of carbonated eclogite at 3.5–5.5 GPa—implications for silicate and carbonate metasomatism in the cratonic mantle. J Petrol egr078. doi:10.1093/petrology/egr078

Klimm K, Blundy JD, Green TH (2008) Trace element partitioning and accessory phase saturation during H_2O-saturated melting of basalt with implications for subduction zone chemical fluxes. J Pet 49:523–553. doi:10.1093/petrology/egn001

Korsakov AV, Hermann J (2006) Silicate and carbonate melt inclusions associated with diamonds in deeply subducted carbonate rocks. Earth Planet Sci Lett 241:104–118

Korsakov AV, Shatsky VS, Sobolev NV, Zayachokovsky AA (2002) Garnet–biotite–clinozoisite gneiss: a new type of diamondiferous metamorphic rock from the Kokchetav Massif. Eur J Miner 14:915–928

Korsakov AV, Theunissen K, Kozmenko OA, Ovchinnikov YI (2006) Reaction textures in clinozoisite gneisses. Russ Geol Geophys 47:497–510

Korsakov AV, Theunissen K, Smirnova LV (2004) Intergranular diamonds derived from partial melting of crustal rocks at ultra-high-pressure metamorphic conditions. Terra Nova 16:146–151

Korsakov AV, De Gussem K, Zhukov VP et al (2009) Aragonite–calcite–dolomite relationships in UHPM polycrystalline carbonate inclusions from the Kokchetav Massif, northern Kazakhstan. Eur J Mineral 21:1301–1311. doi:10.1127/0935-1221/2009/0021-1992

Korsakov AV, Vandenabeele P, Perraki M, Moens L (2011) First findings of monocrystalline aragonite inclusions in garnet from diamond-grade UHPM rocks (Kokchetav Massif, Northern Kazakhstan). Spectrochim Acta Part A Mol Biomol Spectrosc 80:21–26. doi:10.1016/j.saa.2010.12.024

Kostitsyn YA (2007) Relationships between the chemical and isotopic (Sr, Nd, Hf, and Pb) heterogeneity of the mantle. Geochem Int 45:1173–1196. doi:10.1134/S0016702907120014

Kretz R (1983) Symbols for rock-forming minerals. Am Mineral 68:277–279

Kushev VG, Vinogradov DP (1978) Metamorphic Eclogites (in Russian). Nauka, Novosibirsk

Letnikov FA, Kotov AB, Sal'nikova EB, Shershakova MM, Shershakov AV, Rizvanova, NG, Makeev AF (2007) Granodiorites of the Grenville phase in the Kokchetav Block, northern Kazakhstan. Dokl Earth Sci 417:1195–1197. doi:10.1134/S1028334X07080132

Madyukov IA, Chupin VP, Kuzmin DV (2011) Genesis of scapolite from granulites (lower-crustal xenoliths from the Pamir diatremes): results of study of melt inclusions. Russ Geol Geophys 52:1319–1333. doi:10.1016/j.rgg.2011.10.005

Martindale M, Skora S, Pickles J, Elliott T, Blundy J, Avanzinelli R (2013) High pressure phase relations of subducted volcaniclastic sediments from the west pacific and their implications for the geochemistry of Mariana arc magmas. Chem Geol 342:94–109. doi:10.1016/j.chemgeo.2013.01.015

Maruyama S, Parkinson CD (2000) Overview of the geology, petrology and tectonic framework of the high-pressure–ultra-high-pressure metamorphic belt of the Kokchetav Massif, Kazakhstan. Isl Arc 9:439–455

Masago H (2000) Metamorphic petrology of the Barchi-Kol metabasites, western Kokchetav ultrahigh-pressure–high-pressure massif, northern Kazakhstan. Isl Arc 9:358–378

Massonne H (2003) A comparison of the evolution of diamondiferous quartz-rich rocks from the Saxonian Erzgebirge and the Kokchetav Massif: are so-called diamondiferous gneisses magmatic rocks? Earth Planet Sci Lett 216:347–364. doi:10.1016/S0012-821X(03)00512-0

Mazzone P, Haggerty S (1989) Peraluminous xenoliths in kimberlite—metamorphosed restites produced by partial melting of pelites. Geochim Cosmochim Acta 53:1551–1561

McDonough W, Sun S (1995) The composition of the earth. Chem Geol 120:223–253

Mikhno AO, Korsakov AV (2013) K_2O prograde zoning pattern in clinopyroxene from the Kokchetav diamond-grade metamorphic rocks: missing part of metamorphic history and location of second critical end point for calc-silicate system. Gondwana Res 23(3):920–930. doi:10.1016/j.gr.2012.07.020

Mikhno AO, Schmidt U, Korsakov AV (2013) Origin of K-cymrite and kokchetavite in the polyphase mineral inclusions from Kokchetav UHP calc-silicate rocks: evidence from confocal Raman imaging. Eur J Mineral 25(5):807–816. doi:10.1127/0935-1221/2013/0025-2321

Norman M, Griffin W, Pearson N, Garcia M, O'Reilly S (1998) Quantitative analysis of trace element abundances in glasses and minerals: a comparison of laser ablation inductively coupled plasma mass spectrometry, solution inductively coupled plasma mass spectrometry, proton microprobe and electron microprobe data. J Anal At Spectrom 13:477–482

Nozhkin AD, Turkina OM (1993) Geochemistry of granulites of the Kansk and Saryzhalgaisk complexes. UIGGM SO RAN, Novosibirsk

Ogasawara Y, Ohta M, Fukasawa K et al (2000) Diamond-bearing and diamond-free metacarbonate rocks from Kumdy-Kol in the Kokchetav Massif, northern Kazakhstan. Isl Arc 9:400–416

Ogasawara Y, Fukasawa K, Maruyama S (2002) Coesite exsolution from supersilicic titanite in UHP marble from the Kokchetav Massif, northern Kazakhstan. Am Mineral 87:454–461

Parkinson C (2000) Coesite inclusions and prograde compositional zonation of garnet in whiteschist of the HP-UHPM Kokchetav massif, Kazakhstan: a record of progressive UHP metamorphism. Lithos 52:215–233

Perchuk AL, Yapaskurt VO, Podlesskii S (1998) Genesis and exhumation dynamics of eclogites in the Kokchetav massif near mount Sulu-Tjube, Kazakhstan. Geochem Int 36:877–885

Plank T (2005) Constraints from Thorium/Lanthanum on sediment recycling at subduction zones and the evolution of the continents. J Pet 46:921–944. doi:10.1093/petrology/egi005

Plank T, Langmuir C (1998) The chemical composition of subducting sediment and its consequences for the crust and mantle. Chem Geol 145:325–394

Ragozin AL, Liou JG, Shatsky VS, Sobolev NV (2009) The timing of the retrograde partial melting in the Kumdy-Kol region (Kokchetav Massif, Northern Kazakhstan). Lithos 109:274–284. doi:10.1016/j.Lithos.2008.06.017

Rapp R, Watson E, Miller C (1991) Partial melting of amphibolite eclogite and the origin of Archean trondhjemites and tonalites. Precambrian Res 51:1–25. doi:10.1016/0301-9268(91)90092-O

Reverdatto VV, Lepetyukha VV, Kolobov VY (1993) Contact effect of the Zerenda granites on the Berlyk Suite rocks in the Kokchetav anticlinorium. Russ Geol Geophys 34:117

Rollinson HR, Windley BF (1980) Selective elemental depletion during metamorphism of archaean granulites, scourie, NW Scotland. Contrib Mineral Petrol 72:257–263. doi:10.1007/BF00376144

Rozen O (1971) Rifean in the Kokchetav massif. Proc USSR Acad Sci 7:102–104

Rubatto D, Hermann J (2007) Experimental zircon/melt and zircon/garnet trace element partitioning and implications for the geochronology of crustal rocks. Chem Geol 241:38–61

Rudnick R, Barth M, Horn I, McDonough W (2000) Rutile-bearing refractory eclogites: missing link between continents and depleted mantle. Science 287:278–281

Ryerson F, Watson E (1987) Rutile saturation in magmas—implications for Ti-Nb-Ta depletion in island-arc basalts. Earth Planet Sci Lett 86:225–239

Sawyer E (2008) Atlas of migmatites. National Research Council Research Press, Canada

Scherrer N, Gnos E, Chopin C (2001) A retrograde monazite-forming reaction in bearthite-bearing high-pressure rocks. Schweiz Miner Petrogr Mitteilungen 81:369–378

Schertl H-P, Sobolev NV (2013) The Kokchetav Massif, Kazakhstan: "Type locality" of diamond-bearing UHP metamorphic rocks. J Asian Earth Sci 63:5–38. doi:10.1016/j.jseaes.2012.10.032

Schmidt M, Dardon A, Chazot G, Vannucci R (2004a) The dependence of Nb and Ta rutile-melt partitioning on melt composition and Nb/Ta fractionation during subduction processes. Earth Planet Sci Lett 226:415–432. doi:10.1016/j.epsl.2004.08.010

Schmidt M, Vielzeuf D, Auzanneau E (2004b) Melting and dissolution of subducting crust at high pressures: the key role of white mica. Earth Planet Sci Lett 228:65–84. doi:10.1016/j.epsl.2004.09.020

Schnetger B (1994) Partial melting during the evolution of the amphibolite- to granulite-facies gneisses of the Ivrea Zone, northern Italy. Chem Geol 113:71–101. doi:10.1016/0009-2541(94)90006-X

Shatagin K, Degtyarev K, Astakhantsev O (1999) Isotope composition of Sr and Nd in granitoids of the Kokchetav massiv. Dokl Russ Acad Sci 369:525–528

Shatagin K, Degtyarev K, Golubev V, Astakhantsev O, Kuznetsov N (2001) Vertical and lateral heterogeneity of the crust beneath Northern Kazakhstan from geochronological and isotopic-geochemical data on Paleozoic granitoids. Geotectonics 5:26–44

Shatskiy VS, Koz'menko OA, Flitsian YS, Sobolev NV (1990) Partitioning of rare-earth elements in the eclogites of metamorphic rock complexes. Dokl Earth Sci Sect 315:265–269

Shatsky V, Sobolev N, Vavilov M (1995) Diamond bearing metamorphic rocks of the Kokchetav Massif (northern Kazakhstan). In: Coleman R, Wang X (eds) Ultrah. Press. Metamorph. Cambridge University Press, Cambridge, pp 427–455

Shatsky VS, Theunissen K, Dobretsov NL, Sobolev NV (1998) New indication of ultra-high pressure metamorphism in the micas-chists of the Kulet site of the Kokchetav Massif (North Kazakhstan). Geol Geofiz 39:1039–1044

Shatsky VS, Jagoutz E, Sobolev NV, Koz'menko OA, Parkhomenko V, Troesch M (1999) Geochemistry and age of ultrahigh pressure metamorphic rocks from the Kokchetav massif (Northern Kazakhstan). Contrib Mineral Petrol 137:185–205

Shatsky VS, Sitnikova ES, Koz'menko OA, Palessky SV, Nikolaeva I, Zayachkovsky A (2006) Behavior of incompatible elements during ultrahigh-pressure metamorphism (by the example of rocks of the Kokchetav massif). Russ Geol Geophys 47:482–496

Skora S, Blundy J (2010) High-pressure hydrous phase relations of radiolarian clay and implications for the involvement of subducted sediment in arc magmatism. J Pet 51:2211–2243. doi:10.1093/petrology/egq054

Skora S, Blundy J (2012) Monazite solubility in hydrous silicic melts at high pressure conditions relevant to subduction zone metamorphism. Earth Planet Sci Lett 321–322:104–114

Sobolev N, Shatsky V (1990) Diamond inclusions in garnets from metamorphic rocks—a new environment for diamond formation. Nature 343:742–746

Sobolev N, Shatskii V, Vavilov M, Goryainov S (1991) Coesite inclusion in zircon from diamond-containing gneisses of Kokchetav massif—1st find of coesite in metamorphic rocks in the USSR. Dokl Akad Nauk SSSR 321:184–188

Spandler C, Pirard C (2013) Element recycling from subducting slabs to arc crust: a review. Lithos 170–171:208–223. doi:10.1016/j.lithos.2013.02.016

Spandler C, Hermann J, Arculus R, Mavrogenes J (2003) Redistribution of trace elements during prograde metamorphism from lawsonite blueschist to eclogite facies; implications for deep subduction-zone processes. Contrib Mineral Petrol 146:205–222

Stepanov AS (2012) Monazite control on Th, U and REE redistribution during partial melting: experiment and application to the deeply subducted crust.PhD (unpublished) thesis, RSES, ANU, Canberra; https://digitalcollections.anu.edu.au/handle/1885/9432

Stepanov AS, Hermann J (2013) Fractionation of Nb and Ta by biotite and phengite: implications for the "missing Nb paradox". Geology 41:303–306. doi:10.1130/G33781.1

Stepanov AS, Hermann J, Rubatto D, Rapp RP (2012) Experimental study of monazite/melt partitioning with implications for the REE, Th and U geochemistry of crustal rocks. Chem Geol 300–301:200–220. doi:10.1016/j.chemgeo.2012.01.007

Taylor SR, McLennan SM (1985) The continental crust: its composition and evolution: an examination of the geochemical record preserved in sedimentary rocks. Blackwell Scientific Publications, Melbourne, p 312

Terabayashi M, Ota T, Yamamoto H, Kaneko Y (2002) Contact metamorphism of the daulet suite by solid-state emplacement of the Kokchetav UHP–HP metamorphic slab. Int Geol Rev 44:819–830. doi:10.2747/0020-6814.44.9.819

Theunissen K, Dobretsov NL, Korsakov AV, Travin A, Shatsky VS, Smirnova L, Boven A (2000a) Two contrasting petrotectonic domains in the Kokchetav megamelange (north Kazakhstan): difference in exhumation mechanisms of ultrahigh-pressure crustal rocks, or a result of subsequent deformation? Isl Arc 9:284–303. doi:10.1046/j.1440-1738.2000.00279.x

Theunissen K, Dobretsov N, Shatsky V, Smirnova L, Korsakov A (2000b) The diamond-bearing Kokchetav UHP massif in Northern Kazakhstan: exhumation structure. Terra Nova 12:181–187. doi:10.1046/j.1365-3121.2000.00293.x

Tretyakov AA, Kotov AB, Degtyarev KE, Sal'nikova EB, Shatagin KN, Yakovleva SZ, Anisimova IV (2011) The Middle Riphean volcanogenic complex of Kokchetav massif (Northern Kazakhstan): Structural position and age substantiation. Dokl Earth Sci 438:739–743

Turner S, Arnaud N, Liu J, Rogers N, Hawkesworth C, Harris N, Kelley S, Van Calsteren P, Deng W (1996) Post-collision, shoshonitic volcanism on the Tibetan plateau: implications for convective thinning of the lithosphere and the source of ocean island basalts. J Pet 37:45–71

Turkina OM, Letnikov FA, Levin AV (2011) Mesoproterozoic Granitoids of the Kokchetav Microcontinent Basement. Dokl Earth Sci 436:176–180. doi:10.1134/S1028334X11020103

Vavilov MA, Sobolev NV, Shatskiy VS (1993) Micas in diamond-bearing metamorphic rocks of Northern Kazakhstan. Dokl Earth Sci Sect 319A:177–182

Vielzeuf D, Holloway JR (1988) Experimental determination of the fluid-absent melting relations in the pelitic system. Contrib Mineral Petrol 98:257–276. doi:10.1007/BF00375178

Vielzeuf D, Montel J (1994) Partial melting of metagreywackes.1. Fluid-absent experiments and phase-relationships. Contrib Mineral Petrol 117:375–393

Vielzeuf D, Clemens JD, Pin C, Moinet E (1990) Granites, granulites, and crustal differentiation. In: Vielzeuf D, Vidal P (eds) Granulites and crustal evolution, NATO ASI series. Springer, Netherlands, pp 59–85

Volkova NI, Stupakov SI, Babin GA, Rudnev SN, Mongush AA (2009) Mobility of trace elements during subduction metamorphism as exemplified by the blueschists of the Kurtushibinsky Range, Western Sayan. Geochem Int 47:380–392. doi:10.1134/S0016702909040053

Watson EB, Harrison TM (1983) Zircon saturation revisited: temperature and composition effects in a variety of crustal magma types. Earth Planet Sci Lett 64:295–304. doi:10.1016/0012-821X(83)90211-X

Xiong X, Keppler H, Audetat A, Ni H, Sun W, Li Y (2011) Partitioning of Nb and Ta between rutile and felsic melt and the fractionation of Nb/Ta during partial melting of hydrous metabasalt. Geochim Cosmochim Acta 75:1673–1692. doi:10.1016/j.gca.2010.06.039

Zheng Y-F, Xia Q-X, Chen R-X, Gao X-Y (2011) Partial melting, fluid supercriticality and element mobility in ultrahigh-pressure metamorphic rocks during continental collision. Earth-Sci Rev 107:342–374

Zhimulev FI (2007) The tectonics and early Ordovician geodynamic evolution of the Kokchetav HP-UHP Metamorphic Belt. PhD (unpublished) thesis, IGM SO RAN, Novosibirsk

Zhimulev FI, Poltaranina MA, Korsakov AV, Buslov MM, Druzyaka NV, Travin AV (2010) Eclogites of the late cambrian-early Ordovician north Kokchetav tectonic zone (northern Kazakhstan): structural position and petrology. Russ Geol Geophys 51:190–203. doi:10.1016/j.rgg.2009.12.020

Zhimulev FI, Buslov MM, Travin AV, Dmitrieva NV, De Grave J (2011) Early-middle Ordovician nappe tectonics of the junction between the Kokchetav HP–UHP metamorphic belt and the Stepnyak paleoisland arc (northern Kazakhstan). Russ Geol Geophys 52:109–123. doi:10.1016/j.rgg.2010.12.009

Zindler A, Hart S (1986) Chemical geodynamics. Annu Rev Earth Planet Sci 14:493–571